

# Modeling hydropower operations at the scale of a power grid: a demand-based approach

Laure Baratgin<sup>1,2</sup>, Jan Polcher<sup>1</sup>, Patrice Dumas<sup>3</sup>, and Philippe Quirion<sup>2</sup>

<sup>1</sup>LMD/IPSL, École Polytechnique, Institut Polytechnique de Paris, ENS, PSL Research University, Sorbonne Université, CNRS, Palaiseau France

<sup>2</sup>CIREAD, AgroParisTech, CNRS, Ecole des Ponts Paris Tech, CIRAD, EHESS, Nogent sur Marne Cedex, France

<sup>3</sup>CIRAD, UMR CIREAD, F-34398 Montpellier, France

**Correspondence:** Laure Baratgin (laure.baratgin@lmd.ipsl.fr)

**Abstract.** Climate change and evolving water management practices may have a ~~profound~~-significant impact on hydropower generation. While hydrological models have been widely used to assess these effects, they often present some limitations. A major challenge lies in ~~the modeling of~~-modeling the release decisions for hydropower reservoirs, which result from intricate trade-offs, involving power sector dispatch, competing water uses, and the spatial allocation of power generation within the  
5 grid.

To address this gap, this study introduces a novel demand-based approach for integrating hydropower within the routing module of land surface models. First, hydropower infrastructures are ~~placed~~-located in coherence with the hydrological network and links are built between hydropower plants and their supplying reservoirs to explicitly represent water transfers built for hydropower generation. Then, coordinated dam operation is simulated by distributing a prescribed electric demand to be  
10 satisfied by hydropower ~~over~~-across the different power plants ~~on~~-within the power grid, while considering the operational constraints associated with the multipurpose nature of most dams.

To validate ~~our approach, this framework is implemented~~-this approach, we implement the framework within the water transport scheme of a land surface model and ~~assessed~~-assess it with the case study of the French electrical system. We drive the model with a high-resolution atmospheric reanalysis and prescribe the observed national hydropower production as the total  
15 power demand to be met by hydropower infrastructures. By comparing the simulated evolution of ~~the stock in reservoirs to the~~-reservoir stocks to observations, we find that the model simulates realistic operations of reservoirs and successfully satisfies hydropower production demands over the entire period. We also highlight the roles of uncertainties in estimated precipitation and of the limited knowledge of hydropower infrastructure on the estimation of production. Finally, we show that such an integration of hydropower operations in the model improves the simulations of river discharges in mountainous catchments  
20 affected by hydropower.

# 1 introduction

## 1.1 Background and motivation

Hydroelectric power is set to play a pivotal role in numerous power grids in the coming decades, offering low-carbon and dispatchable generation capacity. However, power grids that rely on hydropower production are ~~subject-vulnerable~~ to the unpredictability of weather and climate. Consequently, assessing the potential impact of drought events or climate change on hydropower production is a major concern for the development of resilient energy systems.

Numerous studies (Lehner et al., 2005; Van Vliet et al., 2016; Turner et al., 2017; Zhou et al., 2018; Voisin et al., 2020) have revealed ~~the significant impact~~ significant impacts of climate change on hydropower production in certain regions, including southwestern Europe and France. These studies typically employ global hydrological models (GHMs) or land surface models (LSMs) driven by atmospheric projections generated by global climate models (GCMs) (Turner and Voisin, 2022). These models simulate the regional-scale hydrological cycle, offering gridded assessments of surface runoff and streamflow, which are then used to derive hydropower production estimates.

However, the estimation process from streamflow to hydropower production is challenging for three reasons. Firstly, water can be stored in reservoirs for future use. The timing of reservoir releases is then the result of the management of the power grid and the coordinated operation of other plants across various water catchments. ~~Representing these intricate economic and spatial trade-offs, which drive the operation of hydroelectric reservoirs, in climate models is complex.~~ Secondly, reservoirs that feed hydropower plants are often ~~multi-purpose~~ multipurpose and operated to satisfy other water uses, namely irrigation or tourism. Thirdly, hydropower production can involve inter-catchment water transfers, particularly ~~prevalent~~ in mountainous regions where water is stored at higher elevations before being channeled to power plants located in the valleys. ~~Representing these short-scale processes within regional models poses further complications.~~

Existing studies adopt diverse strategies to represent these complex operations of hydroelectric reservoirs, which are generally categorized into two main approaches (Nazemi and Wheeler, 2015b). On the one hand, simulation algorithms rely on predefined rules to compute reservoir releases. These rules are often a function of reservoir inflow and filling level, inspired by the pioneering work of Hanasaki et al. (2006) (e.g. in MOSART-WM a reservoir scheme used by Zhou et al. (2018); Voisin et al. (2020); Ralston Fonseca et al. (2021)) ~~or~~. They can also be defined based on target curves of water levels from which the release is determined (e.g. in VIC-RES (Dang et al., 2020) used by Chowdhury et al. (2021); Siala et al. (2021)). Such ~~a method~~ accounts ~~methods account~~ for the seasonal behavior of hydroelectric reservoirs, but ~~it misses~~ they miss the representation of short-term operations, as no links with the power system needs are made. On the other hand, optimization algorithms based on the pioneering work of Haddeland et al. (2006) determine the optimal release for each dam. The objective function to optimize varies depending on the reservoir's primary purpose, aiming to maximize individual production for hydroelectric reservoirs. However, ~~these methods consider~~ this method considers each reservoir independently and often ~~employ~~ employs large time steps (monthly) to reduce computational strain.

When the models differentiate the various uses of reservoirs, they categorize the reservoirs based solely on their primary purpose (Abeshu et al., 2023). This approach does not allow ~~for the representation of all the~~ to capture the full range of

55 constraints that apply to most hydroelectric reservoirs, which are often ~~multi-purpose~~multipurpose. Moreover, none of these studies operate the dams as a network that takes advantage of the spatial complementarity of different climatic regions or ~~easading effects~~the cascading effects within river systems.

Finally, none of these large-scale studies explicitly model the water transfers from reservoirs to power plants. In most cases, the flow rate within the grid cell where the power plant is located is used to estimate its production, without considering the actual location of the reservoir (Van Vliet et al., 2016; Zhou et al., 2018; Voisin et al., 2020). ~~However, this~~This approach may lead to an overestimation of production, as the flow rate at the plant site is ~~greater~~higher than at an upstream dam site, and inter-basin transfers may also occur.

## 1.2 Objectives

The objective of this study is to present the original methodology we developed to estimate hydropower production at the scale of a regional power grid. This ~~methodology approach~~ is based on the simulations of a GHM or LSM and addresses the three challenges previously identified: (i) considering the coordinated management of the entire power system at the scale of the power grid; (ii) accounting for the ~~multi-purposes objective~~multipurpose objectives of reservoirs that store water for hydropower production; (iii) representing the inter-catchment water transfers from reservoirs to power plants.

Our approach ~~is inspired by~~draws inspiration from the demand-based algorithms used for irrigation reservoir management, pioneered by Hanasaki et al. (2006). In these algorithms, a demand point (irrigated area) is connected to a supply point (river), with the water demand of the downstream irrigated area driving upstream reservoir releases (Nazemi and Wheater, 2015b; Zhou et al., 2021).

In our methodology, hydropower plants are linked to reservoirs whose releases depend on the demand for hydropower production. At the geographical scale of the whole power grid, the ~~balance between electricity demand and generation is the primary concern~~primary concern is balancing total electricity demand with generation, regardless of the specific locations of consumption and generation. Consequently, we assume that all hydroelectric reservoirs in within the power grid ~~may can~~ contribute to satisfying the demand for dispatchable hydropower production~~defined at the grid level, as a result of the~~, determined by grid-level power system dispatch decisions. Power dispatching involves deciding which types of power plants are activated to satisfy the total power demand, based on the cost and availability of generation resources. ~~We do~~Our model does not explicitly represent this side of the power system decisions but ~~consider a~~uses the corresponding demand for dispatchable hydropower to drive the operation of the hydroelectric reservoirs~~in our model~~.

We implement the proposed methodology in the ORCHIDEE LSM (Krinner et al., 2005), but it aims to be usable in any LSM or GHM. The first steps ~~of~~involve building a river network that represents inter-catchment hydropower transfers and defining rules for reservoir releases. These steps are generic and only require basic information on dam and plant characteristics. To validate the effectiveness of the approach, we apply it to the French power grid. A calibration step is added, which requires more information on individual plants~~to adjust the efficiencies of the power plants~~. Finally, ~~simulated and actual~~the simulated operations of hydroelectric reservoirs are compared with actual operations.

The paper is structured as follows: Sect. 2 describes the proposed methodology and its originality. Sect. 3 introduces the data and methods used for ~~our case study of~~ the French power grid case study and assesses the performance of ORCHIDEE in reproducing river discharges over this area. Sect. 4 ~~details presents~~ the modeling results, and finally Sect. 5 discusses these results and concludes by outlining future perspectives of research.

## 2 Model

Our method relies on three main novelties: building a river network that includes ~~most~~ hydropower-related infrastructures and represents inter-basin hydropower transfers (Sect. 2.1), implementing a reservoir scheme that accounts for ~~multi-purpose~~ multipurpose reservoirs (Sect. 2.2), and using hydropower demand to infer hydroelectric reservoir operations (Sect. 2.3).

### 2.1 Definition of a routing network that includes hydropower connections

The spatial resolution of GHMs or LSMs is typically constrained by the atmospheric grid of the forcing files, which is generally set at  $0.5^\circ$  (approximately 50 km) for large-scale implementations and  $0.1^\circ$  (approximately 10 km) for regional implementations. However, human activities, such as irrigation or urban areas, operate at much ~~higher~~ finer spatial resolutions, typically within a few kilometers. The concept of hydrological transfer units (HTUs) has been introduced in routing modules to bridge ~~the gap between the differing resolutions of atmospheric and hydrological processes resolutions and to provide the opportunity to incorporate human activities in such models this resolution gap~~ (Nguyen-Quang et al., 2018). HTUs correspond to sub-grid river basins, which ~~permit allow~~ runoff generated in one atmospheric grid cell to flow into multiple neighboring ~~atmospheric grid~~ cells. The introduction of these smaller units allows for a more accurate representation of the river system and its interaction with human activities, including hydropower.

Three types of hydropower plants are distinguished, with different implications on locations:

- **Run-of-river plants** ~~lack do not have~~ any storage capacity and generate electricity according to the instantaneous river discharge at the plant location. ~~There is no difficulty involved in the location of the plants;~~
- **Reservoir plants** are fed by reservoirs that can store a specified water volume ~~and are often also used for other~~. These reservoirs often serve multiple purposes, which may constrain the operations of the plant. ~~Electricity~~ The electricity production does not necessarily take place at the location of water storage, therefore the plant and the reservoir need to be located separately ~~∴~~ on the model grid.
- **Poundage plants** are defined in some regions as a subcategory of reservoir plants whose upstream reservoir is relatively small and only allows to store water for a short period.

As an example of different locations of reservoir and power plant, the "La Bathie" power plant, the largest reservoir power plant in France, draws water from the Roselend reservoir, which is located about 20 km away (see Appendix D). At a kilometeric resolution, this implies horizontal water transfers between these two locations (water withdrawal and restitution), which requires the reconstruction of the hydroelectric water supply network within the routing network of ORCHIDEE.

We proceed in three steps, as illustrated in Fig. 1. First (Fig. 1-b), we place dams and hydropower plants on a high-resolution river network (MERIT (Yamazaki et al., 2019) is used in this study), based on geo-referenced data and upstream area provided in infrastructure databases. The location procedure is detailed in Appendix A and the infrastructure datasets used for our study of France are presented in Appendix B. Then, we build the adduction network by identifying supposed connections between power plants and dams that feed them (see Appendix A for more details on the procedure to build the adduction network). Finally (Fig. 1-c), we form HTUs by aggregating MERIT pixels in an atmospheric grid cell with the same general flow direction following the procedures described in Nguyen-Quang et al. (2018) and Polcher et al. (2023).

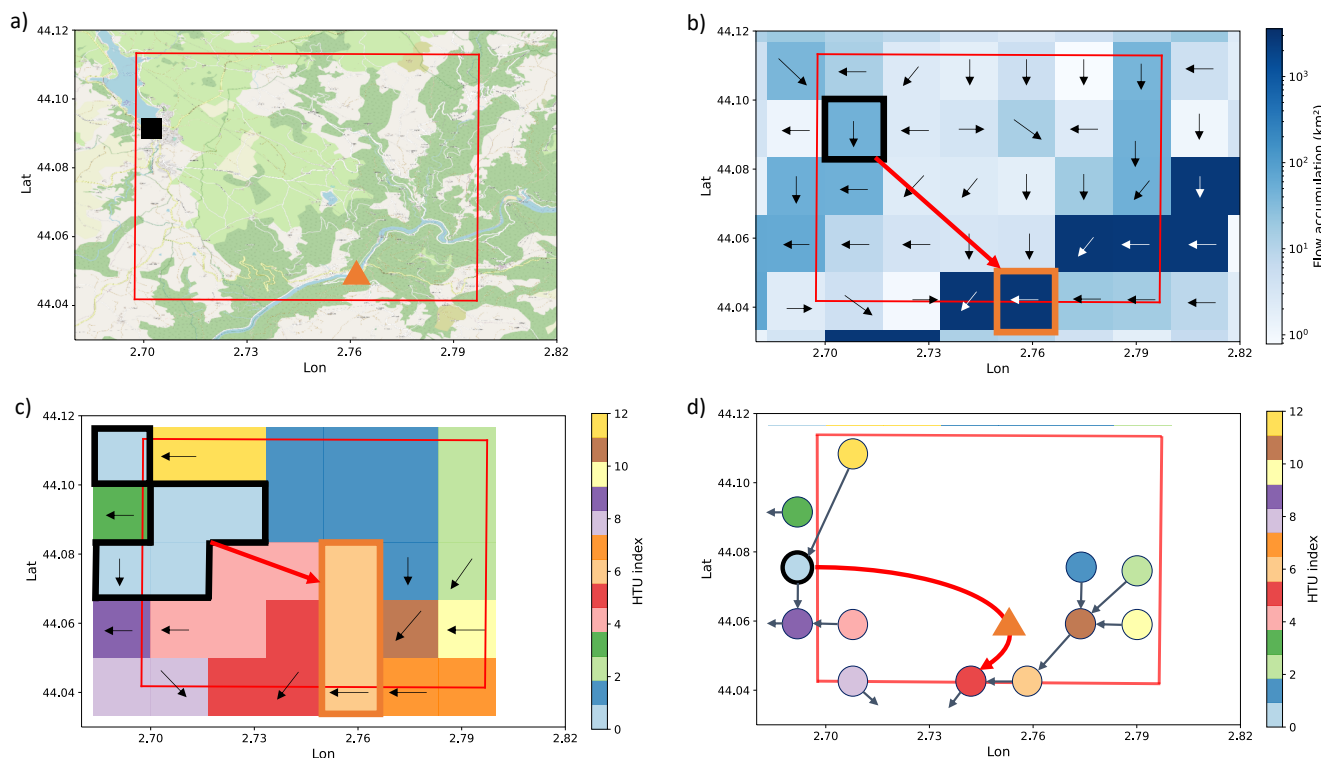


**Figure 1.** Illustration of the procedure to build the ORCHIDEE routing network with using the example of Pouget hydropower plant in France as an example. (a) Geographic context of the Pouget power plant (orange triangle) and its feeding reservoir (black square indicating the location of the dam). The red grid indicates the atmospheric grid. (b) Flow directions and accumulation for the MERIT pixels overlapping the atmospheric grid. The MERIT pixels in which we located the power plant and the dam are respectively indicated in orange and black, while the red arrows represent arrow represents the identified adduction network link we identify. (c) Resulting HTUs-HTU decomposition. The location of the infrastructures is reported in the corresponding HTUs. (d) Corresponding HTUs-HTU graph. The HTU containing the dam is indicated with a bold black outline while the power plant (orange triangle) is placed on the edge between the reservoir HTU and the HTU downstream from the one in which where it has been located.

This procedure results in an HTU network representing natural and human-made water flows. ~~H-This network~~ can be seen as a directional graph (Fig. 1-d) where vertices correspond to HTUs and edges represent directional water flows (both natural and human-made flows for hydropower purposes). ~~Considering~~. In this graph, hydropower plants are placed on the edges connecting the HTU of their withdrawal point and the HTU downstream of the one in which where they are located. Fig. 2 introduces the notation that will be used throughout the article to index HTUs and edges in such graphs. It shows that the water used to produce electricity can follow a different path from the natural flow out of the reservoir. This approach allows for the representation of this distinction independently of the atmospheric resolution.

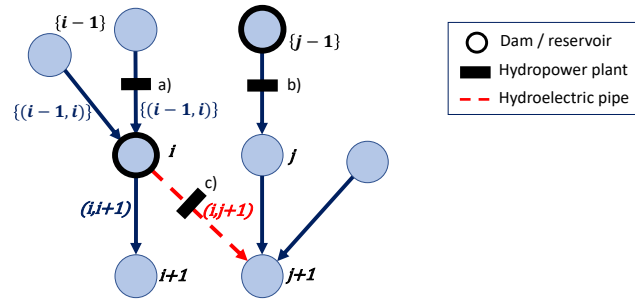


**Figure 2.** Graph representation of the river routing network built. Each vertex represents an HTU. HTUs containing a dam are represented by bold dark circles. Edges represent existing water flow directions (blue edges for natural water flows and dashed red ones for hydroelectric pipes). Power plants are placed on edges whose water flows they can use to produce power ((a): run-of-river plant, (b)-(c) reservoir or pondage plants)). The indexing convention is also presented on the graph, with integers used for vertices and couples of integers for edges.  $i + 1$  is the HTU directly downstream of  $i$  (natural flow) while  $\{i - 1\}$  denotes the ensemble of HTU flowing into HTU  $i$ . Similarly  $(i, i + 1)$  is the natural outflow edge from HTU  $i$  while  $\{(i - 1, i)\}$  represent the ensemble of inflow edges into HTU  $i$ , including basin transfers.

~~Attributes~~The attributes and variables describing the reservoir and hydropower characteristics of each HTU  $i$  and vertex  $(i, j)$  are presented in Table 1.

135 During calibration (see Sect. 2.5), plants for which the identification of a single reservoir conducts to a significant misrepresentation of the plant's hydropower potential are identified and a correction is made by moving the withdrawal point so that it gathers enough water to ensure the observed production is possible.

## 2.2 Dams and reservoir parametrization

140 In the initial version of ORCHIDEE (Polcher et al., 2023), each HTU  $i$  contains three natural water stores, characterized by their time constants (slow aquifer, fast aquifer, and stream storage). To represent water management we add a fourth store to the HTUs in which dams have been located to represent water storage in the reservoir (Fig. 3). This section presents the continuity equation for the water volume in this reservoir.

vertex	$V_{tot,i}$	Total maximum storage capacity of the reservoir located in HTU $i$ ( $m^3$ )
	$V_{elec,i}, V_{recr,i}, V_{irri,i}$	Maximum storage capacity dedicated to respective water uses (hydropower, recreation, and irrigation) ( $m^3$ )
	$H_{dam,i}$	Height of the dam ( $m$ )
	<b><math>V_i(t)</math></b>	<b>Current total volume in the reservoir (<math>m^3</math>)</b>
	$V_{min,i}(t)$	Minimum water volume in the reservoir, it evolves with time to account for recreation uses (see Fig. 5) ( $m^3$ )
	$h_{res,i}(t)$	Water level in the reservoir ( $m$ )
	$A_{res,i}(t)$	Surface of the reservoir ( $m^2$ )
edge	$P_{(i,j)}$	Installed hydropower capacity of the plant located on the edge $(i,j)$ (MW)
	$H_{(i,j)}$	Nominal hydraulic head of the plant, obtained with a full reservoir ( $m$ )
	$Typ_{(i,j)}$	Hydropower plant type (run-of-river, poundage, or reservoir)
	$\eta_{(i,j)}$	Production efficiency of the plant (conversion of potential energy to power)
	$E_{(i,j)}(t)$	Production of the plant (MWh)

**Table 1.** Model attributes and variables describing reservoirs and hydropower. The prognostic variable is distinguished in bold

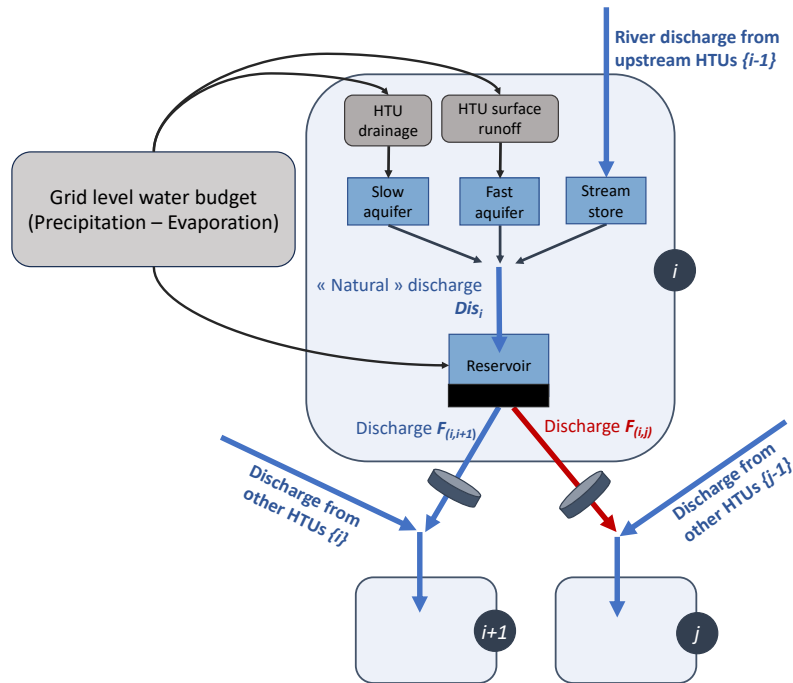


**Figure 3.** Schematic representation of water stores and flows in an HTU  $i$

### 2.2.1 Prognostic equation for water in the reservoir

As represented in Fig. 3, the fast aquifer is filled by local runoff generated in the HTU, the slow aquifer by local drainage  
 145 generated in the HTU, and the stream store by the discharge from upstream HTUs. The equations of these natural water stores  
 are detailed in previous publications (Zhou et al., 2021; Polcher et al., 2023). They introduce the respective time constants of  
 the natural stores  $g_{stream}$ ,  $g_{fast}$  and  $g_{slow}$  (in unit  $h.m^{-1}$ ) and the topographic index calculated for each HTU  $\tau_i$  (in unit  $m^2$ ).

The "natural discharge"  $Dis_i(t)$  in the HTU  $i$  is generated by summing the outflows of the three natural water stores (Eq.  
 (1)). This natural discharge is stored in the reservoir if there is one in the HTU, or routed towards the downstream HTU if there  
 150 is not.

$$Dis_i(t) = \frac{1}{\tau_i} * \left( \frac{W_{stream,i}(t)}{g_{stream}} + \frac{W_{fast,i}(t)}{g_{fast}} + \frac{W_{slow,i}(t)}{g_{slow}} \right) \quad (1)$$

The prognostic equation on reservoir volume is then given by:

$$\frac{dV_i}{dt}(t) = Dis_i(t) + p_{res,i}(t) - ev_{res,i}(t) - \sum_j F_{(i,j)}(t) \quad (2)$$

where  $p_{res,i}(t)$  and  $ev_{res,i}(t)$  are respectively the direct precipitation and evaporation over the reservoir, and  ~~$F_{i,j}(t)$~~   $F_{(i,j)}(t)$   
 155 is the water released from the HTU  $i$  to the HTU  $j$ , which breakdowns as:

$$F_{(i,j)}(t) = \max \left( F_{(i,j)}^{ecol}(t), F_{(i,j)}^{irri}(t), F_{(i,j)}^{elec}(t) \right) + F_{(i,j)}^{spill}(t) \quad (3)$$

Reservoir releases aim at satisfying the different water demands addressed to the reservoir, which are described in Sect. 2.3.  
 Ecological and irrigation releases are limited by the demands addressed to the reservoir and the water available in the reservoir:

$$160 \quad F_{(i,j)}^{ecol}(t) = \min \left( D_{(j,i)}^{ecol}(t), \frac{V_i^*(t) - V_{min,i}(t)}{\tau_{res}} \right) \quad (4)$$

$$F_{(i,j)}^{irri}(t) = \min \left( D_{(j,i)}^{irri}(t), \frac{V_i^*(t) - V_{min,i}(t)}{\tau_{res}} \right) \quad (5)$$

where  $V_i^*(t)$  is the theoretical volume to be obtained without any release (Eq. (6)) and  $\tau_{res}$  is the time constant of the  
 reservoir, which we assume to be of the order of magnitude of a few minutes.

$$165 \quad \frac{dV_i^*}{dt}(t) = Dis_i(t) + p_{res,i}(t) - ev_{res,i}(t) \quad (6)$$

The water released for electricity generation is determined by the production of the plant, computed based on the distribution  
 of the prescribed national demand (see Sect. 2.3).

$$F_{(i,j)}^{elec}(t) = \frac{E_{(i,j)}(t)}{\rho g \eta_{(i,j)} h_{(i,j)}(t)} \quad (7)$$



where  $\rho$  is the water density,  $g$  is the gravitational constant,  $\eta_{(i,j)}$  is the efficiency of the plant (set at 0.9 by default), and  
 170  $h_{(i,j)}(t)$  is the current hydraulic head, which varies with the water level of the reservoir (Eq. (8)).

$$h_{(i,j)}(t) = H_{(i,j)} - (H_{dam,i} - H_{res,i}(t)) \quad (8)$$

Finally, the spillage is defined as the water overflowing without being used for the different uses.

$$F_{(i,j)}^{spill}(t) = \begin{cases} \max\left(\frac{V_i^*(t) - V_{tot,i}}{\tau_{res}} - \sum_k \max\left(F_{(i,k)}^{ecol}(t), F_{(i,k)}^{irri}(t), F_{(i,k)}^{elec}(t)\right), 0\right) & , \text{if } j = i + 1 \\ 0 & , \text{else} \end{cases} \quad (9)$$

Ecological and irrigation flows  $F_{(i,j)}^{ecol}(t)$  and  $F_{(i,j)}^{irri}(t)$  are computed before the other flows, consistently with water manage-  
 175 ment policy in most of the countries.

### 2.2.2 Diagnostic variables

As in previous studies (Fekete et al., 2010; Zhou et al., 2018), we represent each reservoir  $i$  in the form of a tetrahedron of  
 height  $H_{dam,i}$  and volume  $V_{tot,i}$  (Fig. 4).

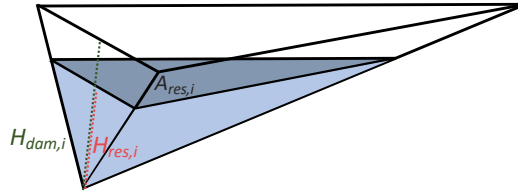


**Figure 4.** Geometry of the reservoir

Hence, the relations between the volume  $V_i(t)$ , the water level  $H_{res,i}(t)$  and the area of the reservoir  $A_{res,i}(t)$  are given by:

$$180 \quad H_{res,i}(t) = H_{dam,i} * \left(\frac{V_i(t)}{V_{tot,i}}\right)^{\frac{1}{3}} \quad (10)$$

$$A_{res,i}(t) = \frac{3 * V_i(t)}{H_{res,i}(t)} \quad (11)$$

Direct precipitation and evaporation ( $m^3/s$ ) over the reservoir are then given by  $p_{res,i}(t) = P_i(t) * A_{res,i}(t)$  and  $ev_{res,i}(t) =$   
 $Ev_i(t) * A_{res,i}(t)$  where  $P_i(t)$  and  $Ev_i(t)$  are respectively the precipitation and evaporation over the HTU  $i$  (in  $m/s$ ).

### 2.3 Water demands

185 Reservoirs are designed to store water for a variety of purposes, including energy production, irrigation, tourism, and domestic  
 and industrial uses. As this study focuses on hydroelectric reservoirs, we adopt a simplistic representation of the other water  
 uses and only consider those that can constrain hydropower operations: ecological flows, irrigation, and tourism.

### 2.3.1 Non-energy demands

In many countries, ~~the~~ environmental laws require a minimum flow  $F_{min,(i,i+1)}$  in the watercourse downstream of a dam in  
 190  $i$ , to guarantee the ecological quality of the river. These ~~minimal flow requirements depend on the region. Details~~ minimum  
 flow requirements vary by region, and specific details for the French study case are presented in Sect. 3.3.1. Such an ecological  
 demand  $D_{(j,i)}^{ecol}(t)$  applies to all reservoirs, regardless of their intended use, and is defined as follows:

$$D_{(j,i)}^{ecol}(t) = \begin{cases} F_{min,(i,i+1)}, & \text{if } j = i + 1 \\ 0, & \text{else} \end{cases} \quad (12)$$

~~Some reservoirs store water for agriculture~~ In addition to ecological requirements, some reservoirs are used for irrigation  
 195 purposes. Water withdrawals for irrigation can be made either directly from the reservoir or from the downstream river. With-  
 draws from the river require ~~a corresponding release~~ corresponding releases from upstream reservoirs to maintain low flows.  
 In this study, the water requirements for irrigation are represented in a highly simplified manner by assuming a need propor-  
 tional to  $F_{min,(i,i+1)}$  during the summer period.  $D_{(j,i)}^{irri}(t)$  is then expressed ~~in Eq. (13). The choice of the as:~~

$$D_{(j,i)}^{irri}(t) = \begin{cases} \alpha_{irri} * F_{min,(i,i+1)}, & \text{if } j = i + 1 \text{ and } V_{irri,i} > 0 \text{ and } t \in Summer \\ 0, & \text{else} \end{cases} \quad (13)$$

200 The proportional factor  $\alpha_{irri}$  and the delimitation of the summer period may vary across regions. Details for ~~our~~ the French  
 case study are presented in Sect. 3.3.1.

$$D_{(j,i)}^{irri}(t) = \begin{cases} \alpha_{irri} * F_{min,(i,i+1)}, & \text{if } j = i + 1 \text{ and } V_{irri,i} > 0 \text{ and } t \in Summer \\ 0, & \text{else} \end{cases}$$

Finally, during the summer months, some reservoirs ~~may also become tourist attractions where recreational activities are  
 carried out and require~~ also serve as tourist attractions, requiring the reservoir to be ~~kept~~ maintained at a high level to  
 205 accommodate recreational activities. To ensure proper reservoir filling during the summer season, dam operators follow a  
 filling guide curve. We define corresponding constraints on  $V_{min,i}(t)$  based on previous ~~work and data available~~ research and  
 available data for French reservoirs (e.g. François (2013) on the Serre Ponçon reservoir), as ~~shown~~ illustrated in Fig. 5. By  
 default, the minimum volume is set at 10% of the total capacity of the reservoir and is increased to 90% during the tourist  
 season for the reservoirs concerned.

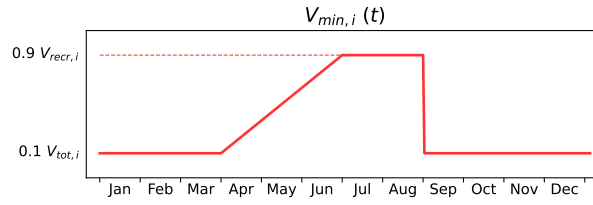


Figure 5. Evolution of the minimum Minimum volume constraints during throughout the year.

### 210 2.3.2 Hydroelectric demand

Production The production of hydropower plants is the result of the dispatch of the total power demand among the different power plants on within the power grid (Stoft, 2002; Wood et al., 2013). Power To meet power demand at minimum cost, power generation units are called upon from least to most expensive to meet power demand at minimal cost. Run-of-river power plants, whose production is free and non-dispatchable, are called upon first, along with solar and wind power plants, to produce to  
215 their maximum potential (as long as it does not exceed total demand, otherwise there is a curtailment of their production). On the contrary, the call upon dispatchable reservoir power plants is the result of a much more complex trade-off, aiming to minimize the total power system cost. From the point of view of perspective of a social planner, in charge of dispatch decisions and aware of the potentials and costs of all the units available in the network area within the power grid, as well as the electricity demand, it is thus possible to define at each time step a demand for dispatchable hydroelectric power hydropower generation  
220  $D_{res}(t)$  can be defined at each time step. This demand (or production target) is defined for the whole grid and needs then to be distributed allocated among the different plants to decide the amount of energy generated  $E_{(i,j)}(t)$  at each plant location, that determine the energy generated at each location  $E_{(i,j)}(t)$ , which will then drive reservoir release decisions. Indeed, knowing  $E_{(i,j)}(t)$ , the model deduces the additional water release needed for the plant production (Eq. (7)) and can finally compute the reservoir release based on Eq. (3).

225 To distribute national demand into individual plants  $D_{res}(t)$  into individual plant production  $E_{(i,j)}(t)$ , the model proceeds in two steps.

**1) Fatal production:** The model starts by going through all the hydropower plants and calculates the energy they can produce or store without additional release, thanks to other releases (ecological or irrigation) or the water expected to overflow. Associated production  $E_{fatal,(i,j)}(t)$  and  $E_{spill,(i,j)}(t)$  are computed based on Eq. (14) and (15).

$$230 E_{fatal,(i,j)}(t) = \min \left( P_{(i,j)} \frac{h_{(i,j)}(t)}{H_{(i,j)}}, \max (F_{ecol,(i,j)}(t), F_{irri,(i,j)}(t)) \times \rho g \eta_{(i,j)} h_{(i,j)}(t) \right) \quad (14)$$

$$E_{spill,(i,j)}(t) = \min \left( P_{(i,j)} \frac{h_{(i,j)}(t)}{H_{(i,j)}} - E_{fatal,(i,j)}(t), \max \left( \frac{V_i^*(t) - V_{tot,i}}{\tau_{res}} - \max (F_{ecol,(i,i+1)}(t), F_{irri,(i,i+1)}(t)), 0 \right) \times \rho g \eta_{(i,j)} h_{(i,j)}(t) \right) \quad (15)$$

The remaining production demand to dispatch is then  $D_{res}(t) - \sum_{Typ(i,j) \in \{poundage, reservoir\}} (E_{fatal,(i,j)}(t) + E_{spill,(i,j)}(t))$ .

235

**2) Reservoirs withdrawals:** If there is any national production demand left to dispatch ( $D_{res}(t) > 0$ ), it should be **produced met** by withdrawing water from the reservoirs. In this study, we consider that the reservoirs are used in the decreasing order of their relative filling **levels** to produce power while respecting production constraints (installed capacity of the plant and the remaining volume of water in the reservoir). The remaining production is dispatched following this rule, until either all remaining production demand **has been satisfied is fulfilled**, or no more plants can produce. This rule leads to the equalization of relative filling **levels** at the end of each time step. This is equivalent to implementing a uniform rule curve for all reservoirs, as has been done in Dang et al. (2020). Another advantage of this rule is that **it leads to a production spread out over the whole hydropower production is distributed across the entire** territory. All plants are required to produce a little power each day, close to the so-called stable productions modeled in other studies (Sterl et al., 2020).

## 245 2.4 Validation diagnostics

The performance of our model to estimate hydropower production will be assessed based on three main diagnostics: the annual hydropower potential (AHP) simulated at each individual plant, the hydraulic stock simulated at the national level, and the time series of simulated production by hydropower plant type.

We define  $AHP_{(i,j)}(y)$  as the maximum energy that could be produced by the plant  $(i,j)$  over the year  $y$  in our simulation. To compute it, we run a simulation in which the demand for dispatchable hydropower  $\overline{D_{res,t}} \overline{D_{res}}(t)$  is fixed to infinite, leading all hydroelectric reservoirs to release water within the limits of water availability and the installed capacity of the plant. The simulated water flow  $F_{i,j}(t)$  at the plant location is then used to compute  $AHP_{(i,j)}(y)$  based on Eq. (16), considering the average head of each plant  $\overline{h_{(i,j)}}$ , which is determined based on Eq. (8), taking the average reservoir water level.

$$AHP_{(i,j)}(y) = \int_{t \text{ in } y} \min\left(\rho g \eta_{(i,j)} \overline{h_{(i,j)}} F_{(i,j)}(t), P_{(i,j)}\right) dt \quad (16)$$

255 The hydraulic stock is the total energy that can be produced using energy stored in all the reservoirs of reservoir plants belonging to the power grid, it is defined by (Eq. (17)).

$$S(t) = \sum_{(i,j) \text{ s.a. } Typ_{(i,j)} = \text{reservoir}} \int_{V_{min,i}(t)}^{V_i(t)} \rho g \eta_{(i,j)} h_{(i,j)}(V) dV \quad (17)$$

Finally, for a hydropower plant type  $k$  (run-of-river or reservoir), the simulated production  $E_k(t)$  is given by:

$$E_k(t) = \sum_{(i,j) \text{ s.a. } Typ_{(i,j)} = k} E_{(i,j)}(t). \quad (18)$$

## 260 2.5 Calibration

A calibration step is performed based on the comparison of simulated AHP and observed production at each individual plant, provided that such data is available. The objective of this step is to identify and correct errors from different sources, which are discussed in this section. The calibration procedure then varies according to the type of power plant.

### 2.5.1 Run-of-river plants

265 ~~A discrepancy~~ Discrepancies between the simulated AHP of a run-of-river plant  $AHP_{(i,j)}(y)$  and its historical production ~~can be attributed to~~  $E_{(i,j)}(y)$  can arise from five factors:

1. ~~A hydro-meteorological bias~~ Hydro-meteorological biases of the model may result in discrepancies in river discharges between the model and the actual river conditions;
2. An inexact location of the ~~hydropower plants during the placement plant~~ on the HTU graph may lead to inaccurate ~~estimations~~ estimates of the available discharge at the plant's location;
- 270 ~~We assume~~ The model assumes that the plant can harness the entire river volume. In reality, the river ~~can be divided~~ may split into several branches, with only one ~~of them passing~~ channeling water through the plant;
4. ~~Plants efficiencies are assumed to be equal~~ A uniform efficiency of 0.9 is assumed for all plants ~~and constant to 0.9~~. ~~In reality, the efficiency of a hydropower plant depends~~. However, actual efficiency varies depending on the type of hydroelectric turbine ~~that is~~ used (the choice is made based on the plant's rated head and flow) and ~~varies with the flow rate~~ flow conditions;
- 275 5. We assume that ~~plants produce at their~~ the plant produces at its maximum potential. ~~However, in reality, a plant~~ In practice, it may be unavailable for ~~a period of time due to maintenance~~. Moreover, maintenance and some of the plant's potential can be reserved for ancillary services to the grid or curtailed if ~~the non-dispatchable~~ potential production of ~~renewables~~ renewable generation potential exceeds the power demand. This can reduce the actual production compared to the potential.
- 280

As in previous studies (Wagner et al., 2017; Zhou et al., 2018), the unknown efficiency of the power plant  $\eta_{(i,j)}$  is adjusted to calibrate the model ~~to the~~ against historical annual generation data ~~based on~~, based on the previously estimated bias (Eq. (19)). Such calibration corrects the total error without differentiating its source.

$$285 \quad \eta_{(i,j)} = \frac{1}{0.9} * \frac{E_{(i,j)}(y)}{AHP_{(i,j)}(y)} \quad (19)$$

### 2.5.2 Poundage and reservoir power plants

Over a year, all the water entering the reservoir  $i$  of a plant  $(i,j)$  could either contribute to the annual production of the plant  $E_{(i,j)}(y)$ , to the annual change of the hydraulic stock in the reservoir  $\Delta S_i(y)$  or spill without generating power.

As for run-of-river plants, differences in simulated AHP and observed production can have different sources. In addition  
290 to the five errors listed above, a sixth possible error, related to the adduction network, should also be considered. Indeed, we  
assume in our model that each plant is only fed by one reservoir, which can lead to an underestimation of the plant production  
if some other water inputs are non-negligible. To account for these different error sources, we calibrate the model in two  
successive steps:

- Step 1: Dams with a large negative bias (inferior to -50 %) are shifted downstream from their original location to take  
295 into account the computed deviation. This ~~can be interpreted as the addition of water inlets~~ adjustment can be seen as  
adding water intakes for the power plant based on the topography, such that the power plant receives enough water.  
Most concerned areas are located in mountains, where the water intakes are quite close geographically (on the same  
atmospheric grid) and therefore subject to the same precipitation, which allows us to assume that the water available per  
unit of area is similar.
- 300 – Step 2: ~~Once the network error is corrected~~ For the other plants, the efficiencies ~~of the plants~~ are adjusted to match the  
observed production, as with run-of-river (Eq. (19)).

### 3 Data and methods for the test case over France

#### 3.1 ORCHIDEE setup

In this study, ORCHIDEE is run in stand-alone mode, forced with the SAFRAN meteorological ~~data set~~ dataset (Quintana-  
305 Segui et al., 2008). SAFRAN (Système d'Analyse Fournissant des Renseignements Atmosphériques à la Neige) is a surface  
reanalysis resulting from the optimal interpolation between the vertical profiles of the atmosphere derived from ERA-40 atmo-  
spheric reanalysis and surface observations. It provides the required atmospheric variables - temperature, relative humidity at  
two meters, wind speed, downward radiation (shortwaves and longwaves), and precipitation (solid and liquid) - at an hourly  
time step over an  $8 \times 8$  km grid that covers France and upstream part of its catchments beyond its borders.

310 To estimate the sensitivity of ORCHIDEE's simulations to the uncertainties of precipitation, we built two alternative atmo-  
spheric forcings by replacing precipitation data in SAFRAN with other precipitation datasets: COMEPHORE (Tabary et al.,  
2012) and SPAZM (Gottardi et al., 2008). These datasets are presented in detail in Appendix C1 and their relative differences  
with SAFRAN are displayed in Fig. C1.

COMEPHORE dataset provides observations of surface precipitation accumulation over metropolitan France at an hourly  
315 and kilometric resolution based on a synthesis of radar and rain gauge data. We build a meteorologic dataset SAF\_COM by  
replacing precipitation data in SAFRAN with data from COMEPHORE. As COMEPHORE does not distinguish solid and  
liquid precipitations, we keep SAFRAN's hourly ratio of solid/liquid precipitations when possible and discriminate based  
on the air temperature otherwise. The differences in annual mean precipitation between SAFRAN and COMEPHORE are  
generally small, with an average deviation inferior to 1.0% ~~in COMEPHORE compared to SAFRAN~~ (Fig. C1). However,  
320 we find a small seasonal bias as this average deviation ~~goes ranges~~ from -2.0% ~~for the Winter period in winter~~ to +1.9%

in ~~the Summer~~summer. Moreover, discrepancies increase dramatically in mountainous regions, especially in the Alps and in the Pyrenees. For grid points with an average elevation above 1000m, the annual mean precipitation in COMEPHORE is, on average, 10.4% lower than in SAFRAN.

325 SPAZM is a daily reanalysis of precipitation at the kilometer scale, developed by EDF, ~~the France's~~main electricity producer ~~in France~~. We interpolate the daily precipitation data from SPAZM to the hourly scale and merge it with SAFRAN data to create the alternative forcing dataset SAF\_SPAZM. As for SAF\_COM, we keep SAFRAN's hourly ratio of solid/liquid precipitations when possible. Compared to SAFRAN, ~~precipitations are~~SPAZM's precipitations is on average 2.7% higher ~~in SPAZM with an average~~, with a bias of 7.0% in ~~Summer, against summer~~ and 2.1% in ~~Winter. Bias~~winter. The bias is heterogeneously spread over France (Fig. C1) with ~~bigger larger~~ differences on the highest reliefs, without a clear sign (~~average deviation of~~  
330 For grid points above 1000 meters, the average deviation is +3.9% ~~for grid points above 1000m~~).

Appendix E provides an extensive assessment and discussion of hydro-meteorological biases in ORCHIDEE simulations over French rivers. In particular, we identified uncertainties in observed precipitation as a main contributor to the error in simulated discharge, especially in the mountains.

335 The vegetation distribution map used in ORCHIDEE is derived from the ESA-CCI Land Cover dataset at 0.05° resolution for the year 2010. The soil background albedo map is derived from the MODIS albedo dataset aggregated at 0.5° resolution. Soil texture distribution maps are obtained from Reynolds map (Reynolds et al., 2000) at 5-arc-min resolution with 12 USDA soil texture classes (at 30 cm depth). In this study, ORCHIDEE performs the energy and water budgets at a 15-minute time step ~~and hydropower~~, and reservoir operations are performed at the same time step. Given that the time step is greater than the time constant of reservoirs, we consider that reservoir spillage always occurs within a single time step.

## 340 3.2 Hydroelectric infrastructure

The infrastructure datasets are presented in detail in Appendix B. We use reservoir data from GRanD (~~Global Reservoirs and Dams~~) (Lehner et al., 2011) and CFBR (CFBR, 2021) datasets. ~~Data~~The data provided in these datasets allow us to validate the assumption about reservoir geometry (Fig. 4). For hydropower plants, we use data from ~~the EU Joint Research Center hydropower plants database (European Commission and Joint Research Centre (JRC), 2019)~~European Commission and Joint Research C  
345 and national registers of electricity generation and storage facilities published annually by the French ~~TSO~~transmission system operator (TSO) (ODRÉ, 2016, 2018).

Following the procedure outlined in Fig. 1, we locate the infrastructures on the MERIT river network and construct the ~~HTUs~~HTU routing graph based on the simplification of this MERIT network (resolution of 2km) on the SAFRAN atmospheric grid (resolution of 8 km). ~~HTUs area~~HTU areas can thus theoretically vary from 0 to 64  $km^2$  and the average area of HTUs in our  
350 graph is 4.73  $km^2$ . The upstream area of an HTU is defined recursively as the sum of the HTU area and the upstream area of all its tributaries. For each hydroelectric infrastructure, we compare in Fig. 6 its reference upstream area (from the database or MERIT network) to the upstream area of the HTU in which it is located. For most of the structures, the positioning error is lower than 20%. Some dams with a small upstream area are, however, located in HTUs with a higher upstream area, due to resolution constraints.

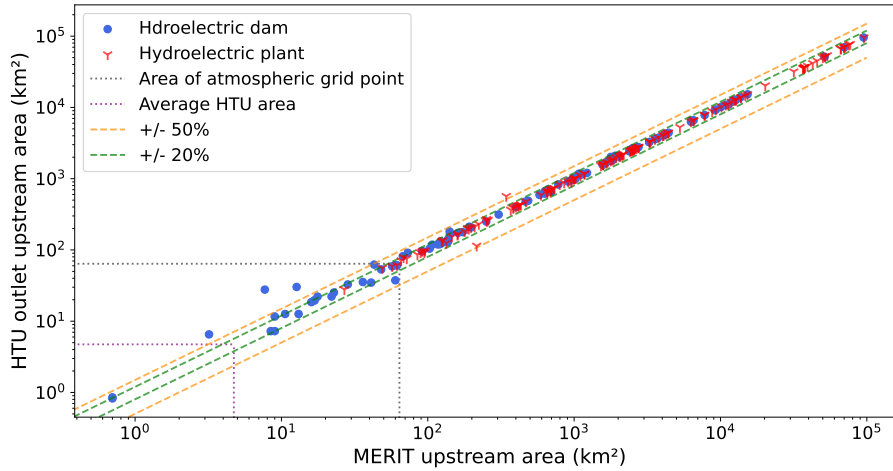


**Figure 6.** Comparison of the initial upstream area of the infrastructure (referenced in the database or upstream area of the MERIT pixel on which it is placed) with its final upstream area in the [HTUs-HTU](#) graph. Blue dots represent hydroelectric reservoirs (reservoirs that have been associated with power plants during the adduction network building step) and red signs represent hydropower plants. Green and orange dashed lines delineate a respective error of +/- 20% and +/- 50% ,while grey and purple dotted lines [respectively](#) refer to the [respective area of an atmospheric grid point area](#) and [the average area of an HTU](#).

### 355 3.3 Data for water demands and validation

#### 3.3.1 Ecological and irrigation demands

In France, [minimal minimum](#) flow requirements are defined relatively to the mean interannual flow [upstream-downstream](#) of the dam  $\overline{Dis}_i$  ([Code de l'Environnement, Article L214-18](#)). They are summarized in Table 2. We ran a twenty-year SAFRAN simulation without reservoir operations to calculate  $\overline{Dis}_i$  at dam locations.

	$\overline{Dis}_i > 80m^3/s$	$\overline{Dis}_i < 80m^3/s$
Dam intended for hydropower purpose	$F_{min,(i,i+1)}(t) = 5\% * \overline{Dis}_i$ or flow immediately upstream of the dam if it is lower	$F_{min,(i,i+1)}(t) = 5\% * \overline{Dis}_i$ or flow immediately upstream of the dam if it is lower
Dam intended for other purpose	$F_{min,(i,i+1)}(t) = 5\% * \overline{Dis}_i$ or flow immediately upstream of the dam if it is lower	$F_{min,(i,i+1)}(t) = 10\% * \overline{Dis}_i$ or flow immediately upstream of the dam if it is lower

**Table 2.** French legal requirements for ecological flow,  $\overline{Dis}_i$  is the mean interannual flow downstream of the dam

360 To account for the irrigation purposes of some reservoirs, we increase the [minimal minimum](#) flow requirement downstream of reservoirs intended for irrigation during the summer period (June 1st to September 30th) by setting  $\alpha_{irri} = 8$ . This choice is based on information available from French reservoir concession contracts, which sometimes specify the volume of water



reserved for irrigation. In the case of Serre-Ponçon, for example, the concession contract stipulates a reserve of 200 million  $m^3$ , to be used for irrigation, between July 1 and September 30. If we consider a constant withdrawal spanning three months, this corresponds to a  $25m^3/s$  flow, which is 45% of the  $55m^3/s$  mean interannual flow at this location, and thus 9 times larger than  $F_{min}$ , which is set to 5%, as explained above.

### 3.3.2 Hydropower production demand

As this study aims to validate our proposed reservoir operations model, we take the historical time series of production as the hydropower demand prescribed to the model. We can thus assess ~~if the reservoir operations performed by the model when it is forced whether the model, when driven~~ by the historical atmospheric dataset, can meet the observed production. ~~Data of levels, Data on~~ observed production for hydropower plants in the French power grid are ~~published available~~ from 2015 onwards ~~by the French electricity transmission system operator RTE, published by RTE, the French TSO,~~ at a 30-minute time step for 2 categories of plants (RTE, a):

- **River production**  $D_{river,t} D_{river}(t)$  that gathers the production of pure run-of-river power plants and poundage power plants (reservoir plants with a storage below 400h)
- **Reservoir production**  $D_{res,t} D_{res}(t)$  that gathers the production of reservoir power plants with a greater storage capacity

In our model,  $D_{river,t} D_{river}(t)$  is then used to drive the production of run-of-river and poundage power plants, while  $D_{res,t} D_{res}(t)$  is used for the reservoir power plants with greater storage capacity, both using the method described in 2.3.2. We use the classification established by RTE and illustrated in Fig. B2.

### 3.3.3 Validation data

In France, ~~hydroelectricity is produced hydropower reservoirs are managed~~ by companies that do not share ~~precise data on the production of their power plants or the filling of the reservoirs they manage~~ ~~detailed data on their production or their filling level~~. Similarly, discharge data from gauging stations near hydroelectric power plants are often ~~inaccessible to the public not publicly accessible~~. This limits the ~~available data data available~~ for validating our model.

However, as a delegate of public services, RTE provides ~~some~~ data, often aggregated at the national level, which allows us to calibrate and validate our model as shown in the following two sections.

The available data ~~is~~ are:

- National time series of production by hydroelectric sector (river and reservoir) at 30-minute time step from 2015 (RTE, a) - which are the time series used for the hydropower production demand;
- Annual production of each hydroelectric power plant for the years 2015, 2016, and 2018 (ODRÉ, 2015, 2016, 2018);
- Weekly hydraulic stock (Eq. (17)) at national level from 2014 to 2020 (RTE, b);

As mentioned in Appendix B, our ~~final hydropower plants~~ hydropower plant dataset does not ~~include all the hydropower plants installed~~ cover all the installed plants in France. However, by using annual production data of each plant provided by (ODRÉ, 2015, 2016, 2018), we can ~~quantify estimate~~ the share of the national production provided by the power plants in our  
395 database. This ~~enables allows~~ us to compute a factor ~~to convert the actual production of~~ for converting the production from national time series (RTE, a) into representative production ~~in our model~~ within our model, both for prescribing the production demand and comparing the results. The calculation of such conversion factors is presented in Table B2.

We also compute the ~~maximal maximum~~ hydraulic stock of the reservoirs associated with the power plants in our database using Eq. (17) and data from our plants and reservoirs databases. We obtain  $S_{max} = 3.66 TWh$ , which is quite close to the 3.59  
400  $TWh$  value reported by RTE (RTE, b). Therefore, we can consider that our database covers all the available storage and that missing hydropower capacity is linked to negligible reservoirs.

## 4 Results

### 4.1 Calibration

We present here the application of the calibration process to the French study case. ~~We assess the discrepancy~~ First, we assess  
405 the discrepancies between the AHP simulated by the model (Eq. (16)) ~~and~~ the observed annual production at each power plant for the years with available data. ~~The~~ We then discuss the likely origin of these discrepancies ~~is then discussed~~. Finally, the calibration process is validated by comparing annual potentials simulated in ORCHIDEE to the observed annual production at the national level for an extended period (~~data available, using data~~ from 2000 to ~~2020~~) 2020. We choose to use SAFRAN forcing as a reference for the calibration step, as this dataset is widely used in regional studies of France.

#### 4.1.1 Discrepancies between AHP and the historical production

Figure 7 shows the average relative bias ~~in of~~ simulated AHP compared to observed production for the three years with available data for the the run-of-river plants in our database. For ~~the majority of most~~ plants, the bias in hydropower potential is comparable to the bias in river discharge computed at ~~neighboring stations~~ nearby stations, which is displayed in Fig. E1; ~~indicating that it mainly comes from the~~. This indicates that the bias mainly stems from hydro-meteorological ~~error errors~~  
415 (reason 1 of the list presented in Sect.2.5). At the Caderousse and Gambsheim power plants, located in Fig. 7, a stronger positive bias is found. At these locations, only part of the river passes flows through the plant, which ~~may contribute to the~~ observed explains the computed bias (reason 3). The calibration leads to obtained efficiencies ranging from 0.43 to 1.31 with a median value of 0.88.

Over a year, ~~all~~ the water entering the reservoir of a reservoir or poundage power plant ~~could can~~ either contribute to the  
420 annual production of the plant  $E_{(i,j)}(y)$ , to the annual change ~~of in~~ the hydraulic stock ~~in within~~ the reservoir  $\Delta S_i(y)$ , or spill without generating power. Observed production  $E_{(i,j)}(y)$  is available for the three years mentioned earlier; ~~however~~ observations of the change of the. However, observations of changes in the hydraulic stock are only available at the national

Mean relative bias of simulated AHP compared to observed annual production  
Run-of-river plants

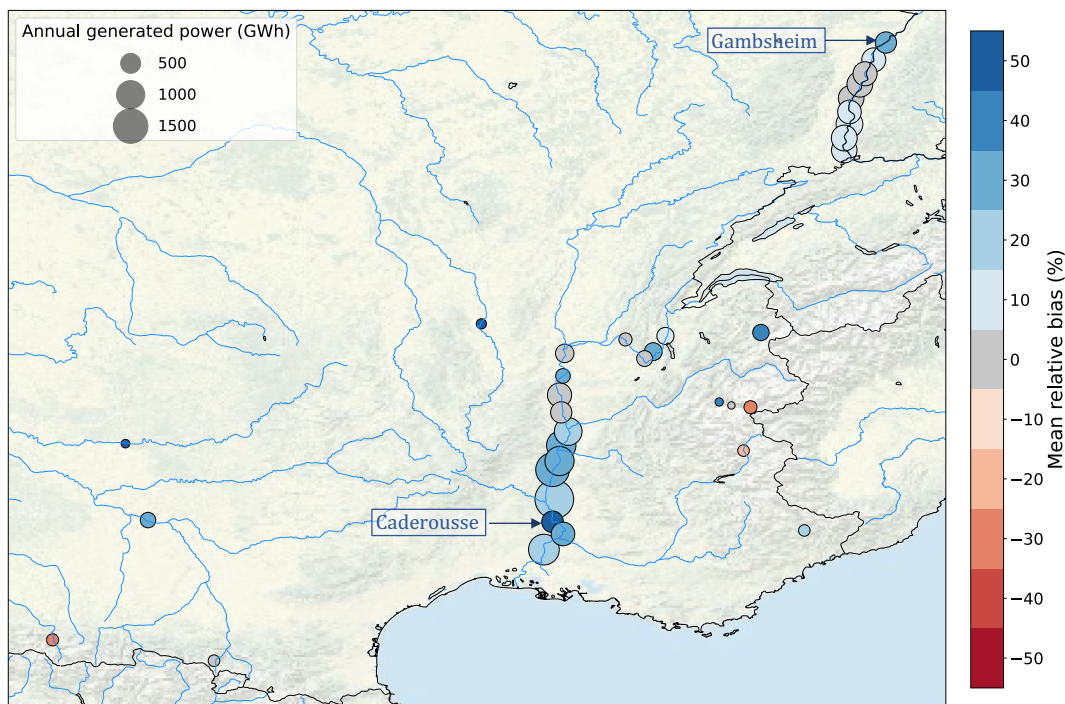


**Figure 7.** Average relative bias of simulated ~~annual hydropower potential~~ AHP compared to observed ~~historical annual~~ production for run-of-river power plants with available data. The point size corresponds to the average annual production.

Source: ~~authors~~ Authors, based on a layer by U.S. National Park Service

level, for the national stock  $\Delta S_{obs}(y) = \sum_{i \text{ in res}} \Delta S_i(y)$ . To compare simulated AHPs with observations of production and stored energy, we make the two following assumptions: (i) spillages that do not produce power can be neglected, and (ii) the ~~change-changes~~ in the hydraulic stock ~~is-are~~ homogeneous across all reservoirs:  $\forall i, \Delta S_i(y) = \Delta S_{obs}(y) \times \frac{S_{max}}{S_{i,max}}$ . In Fig. 8, we plot the average bias of  $AHP_{(i,j)}(y)$  relative to observed net production  $E_{(i,j)}(y) + \Delta S_i(y)$  for the three years for which data ~~is-are~~ available. It enables us to distinguish two types of bias in the simulated AHP, suggesting that two main error sources can be distinguished:

- Plants ~~that have with~~ an absolute bias inferior to 50% (represented by circles in Fig. 8). Their biases are generally similar to ~~the one those~~ of discharge for ~~neighboring stations~~ nearby stations, displayed in Fig. E1.
- Plants ~~that have with~~ a bias inferior to -50% (represented by pentagons in Fig. 8). These plants are mainly located in ~~mountain~~ mountainous areas and have a negative bias ~~larger than the one~~ stronger than that of the discharges in ~~this the~~ area. Moreover, their biases have a small interannual variance, indicating that the error is stable ~~in-over~~ time (not shown).

## Mean relative bias of simulated AHP compared to observed annual production Reservoir plants

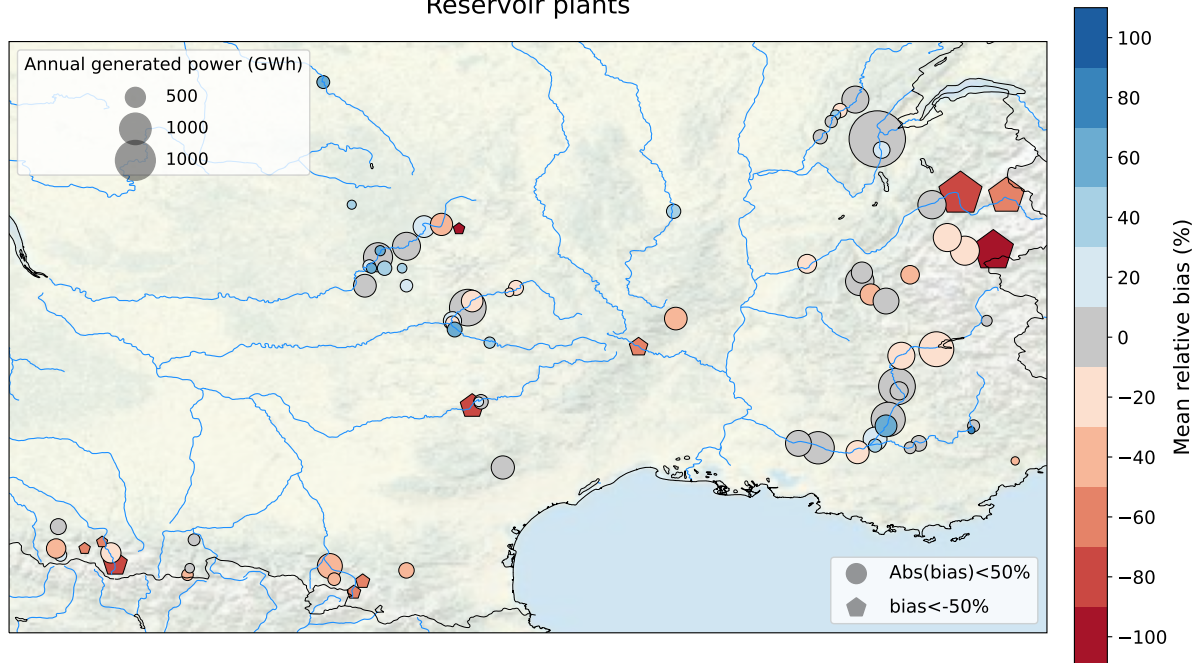


**Figure 8.** Average relative bias in the of simulated AHP compared to the observed historical net annual production of for reservoir and poundage power plants with available data. The point size corresponds to the average annual production of the plant.

Source: authors Authors, based on a layer by U.S. National Park Service

### 4.1.2 Validation of the calibration

435 The performance of the calibrated model is assessed by comparing the potentials simulated by the calibrated model forced by SAFRAN with the historical annual production (RTE, a) for the different categories of power plants at the national scale over the whole period 2010-2020. We assume that hydropower is used as much as possible and that the production is well managed so that the AHP is a good proxy to compare with the actual production. For a given For each plant category, the simulated annual potential is computed by summing the AHP of all plants belonging to within this category. For poundage and reservoir  
440 plants, we directly compare this aggregated potential to the historical production, as stock data (RTE, b) is are not available for the whole period. This relies on the assumption that the national stock returns to its initial value at the end of each year.

The calibration appears to be robust as a very small bias very small biases (less than 3%) is are obtained when comparing the simulated potentials to the observed production (Fig. 9). The relative differences in annual production are on average lower than 10%. This indicates that the model is able to capture the overall pattern of interannual variability of the observed production.

445 We also explore the sensitivity of our the model and calibration procedure to the uncertainties in precipitation forcings that are highlighted in Fig. C1 and E2. We compute AHPs under the two alternative forcings (Fig. 9) and compare the obtained

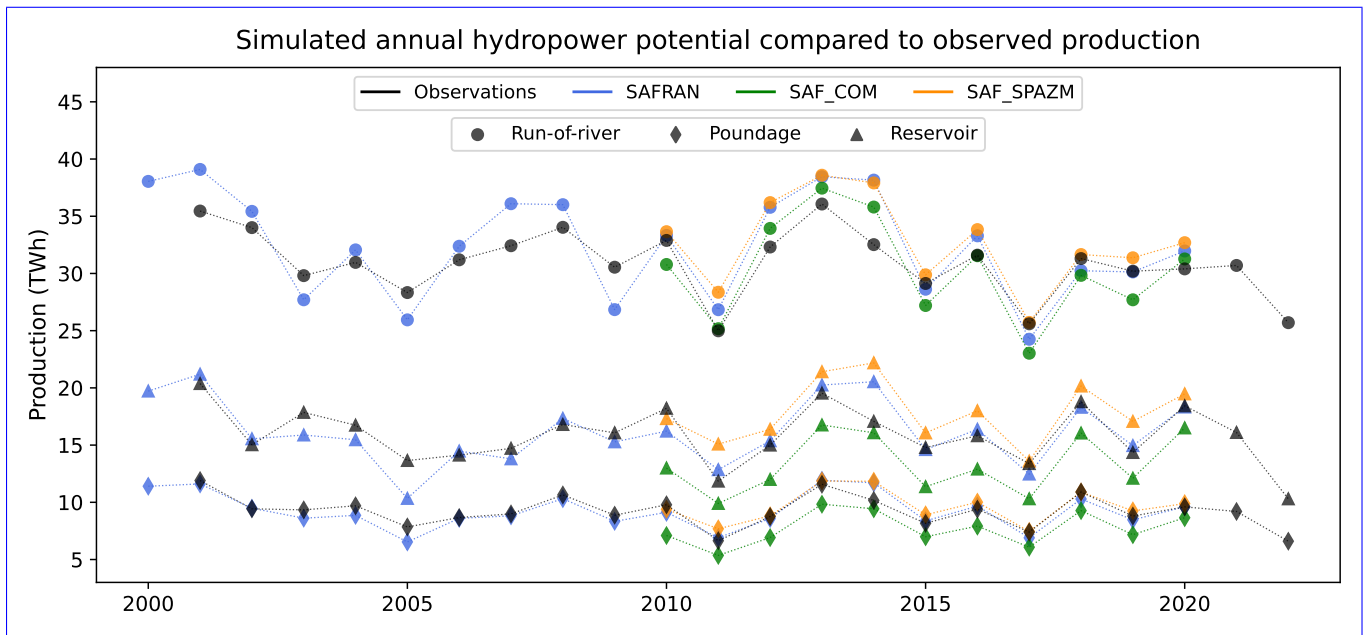


**Figure 9.** Comparison of estimated annual hydropower potential with observed annual production for the different categories of hydropower plants and for the different atmospheric forcings, after calibration based on SAFRAN.

inter-forcing variability with the inter-annual variability of observed production ~~to the inter-forcing variability~~ (Tab. 3). Run-of-river annual potentials exhibit little variation across the different forcings, as the simulated flows of major rivers hosting run-of-river power plants (primarily the Rhone and the Rhine) demonstrate a low sensitivity to precipitation uncertainty (see Fig. E3). Consequently, the inter-forcing variability of simulated potential (~~defined as the mean standard deviation of annual potential across the forcings~~) is three times smaller than the interannual variability of run-of-river power production (~~defined as the standard deviation of observed annual productions~~), see Table 3). It is also slightly smaller than the modeling error (~~RMSE of SAFRAN simulated potentials compared to observations~~), indicating a low sensitivity of simulated run-of-river production to the precipitation uncertainty. Conversely, reservoir plant production shows a much higher sensitivity to precipitation disparities between forcings. Lower COMEPHORE precipitations in mountainous regions lead to an average decrease of 18.7% in the total simulated potential, compared to the SAFRAN simulation. As a result, the variability among forcings is of the same order of magnitude as the interannual variability of production and is higher than the modeling error. Finally, poundage power plants fall in an intermediate category, displaying an inter-forcing variability that is 41% lower than the interannual variability.

In conclusion, the uncertainties in precipitation forcing in mountainous regions prove to be critical in the estimation of realistic hydropower potentials for reservoir plants. The calibration carried out relative to SAFRAN is less effective for other forcings, SAF\_COM for instance, as the differences in precipitation data appear as the main contributor to the differences in hydropower potentials.

Comparison of estimated annual hydropower potential with observed annual production for the different categories of hydropower plants and for the different atmospheric forcings, after calibration based on SAFRAN.

465

	Run-of-river		Poundage		Reservoir	
	Calibration Period	Validation Period	Calibration Period	Validation Period	Calibration Period	Validation Period
Mean relative error	-	+ 2.8 %	-	-2.6 %	-	-1.4 %
Mean absolute relative error	3.5 %	6.9 %	3.7 %	5.4 %	2.5 %	7.5 %
Interannual variability (TWh) <sup>a</sup>	3.71		1.71		2.61	
Inter-forcing variability (TWh) <sup>b</sup>	1.32		1.25		2.54	
Modeling error (TWh) <sup>c</sup>	2.64		0.67		1.33	

<sup>a</sup> We define the interannual variability daily as the standard deviation of observed annual productions.

<sup>b</sup> We define the inter-forcing variability as the mean standard deviation of annual potential across the forcings.

<sup>c</sup> We define the modeling error as the RMSE of SAFRAN simulated potentials compared to observations.

**Table 3.** Estimation of the errors in annual potentials prediction

## 4.2 Hydropower operations

470

In this section, we assess the model's ability to simulate reservoir management and hydropower production. Observed time series of river production (gathering run-of-river and poundage power plants) and reservoir production serve as demand inputs for the reservoir operations in the model. At each time step, the model aims to meet this target by operating the reservoirs according to the rules described in Sect. 2.3 and the simulated hydrological cycle. The objective is to verify if our model can simulate operations consistent with observed production. We present here the results obtained from a simulation spanning the period from 2015 to 2020.

### 4.2.1 River production

475

At each time step, the model first computes the available potential from fatal production (from run-of-river plants and spill or constrained releases from the reservoirs of poundage plants). If this potential falls short of fulfilling the production target, ~~it the~~ model then operates the reservoirs ~~associated~~ connected with poundage plants to supplement the production.

480

Figure 10 details how the simulation compares to the prescribed production ~~throughout over~~ the period when the model is forced by SAFRAN. The model successfully reproduces the overall seasonality of ~~the production is quite well reproduced, with the model succeeding in production,~~ meeting the hourly production target 69.0% of the time. The failures (in red in Fig. 10) ~~represent a total volume of account for~~ 6.9% of the prescribed production over total prescribed production across the six years. They mostly occur during summer and fall ~~and indicate,~~ indicating that the simulated hydrology is unable to produce what was actually produced during these periods. In winter and spring, ~~however on the contrary,~~ there are instances when the potential

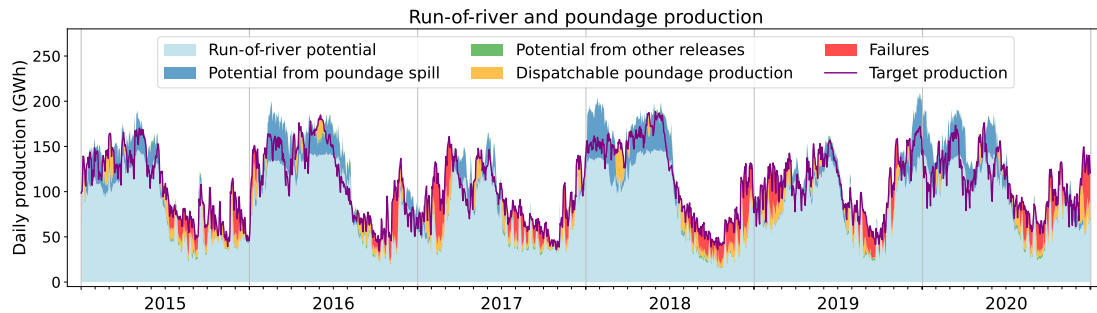


**Figure 10.** Run-of-river Daily production from run-of-river and poundage plants daily production. The purple line indicates the production prescribed to the model and the red coloring shows the failures of the model to meet this target production, when the model is forced by SAFRAN. The other colors refer to the nature of the flow that contributes to production in the model simulated production. Light blue represents the gross potential of run-of-river plants, dark blue represents the potential of from spill from poundage reservoir (water overflowing from the reservoir), green represents the potential from constrained releases of from poundage reservoirs; and lastly orange represents the dispatchable production, generated by the water specifically released from the poundage reservoirs for power generation.

of fatal production is higher than exceeds the target production (January and February 2018 for instance), which means that, in the model, more power could have been generated. This means that the model could have generated more power during these periods than was actually observed produced. These discrepancies are likely due to the discharge seasonality bias in discharge within the Rhone and Rhine catchments, as highlighted in Fig. E4. Despite these discrepancies, the performance of the model remains satisfactory, as it captures the gross seasonality and magnitude of run-of-river production, in addition to the inter-annual variability (Fig.9).

Simulation of The run-of-river production in the model, simulated by the model when forced by the alternative forcings SAF\_SPAZM and SAF\_COM, are presented in Fig. C2 and C4. Using SAF\_SPAZM, the failures in meeting the prescribed production are reduced (4.3% of production not satisfied compared to 6.9%); due to slightly higher annual potentials of run-of-river and poundage power plants (Fig. 9). On the other hand, higher failures are obtained with SAF\_COM the lower potentials lead to higher failures (15.4% of the total production), consistent consistently with the lower potentials obtained in Fig. 9. However, the seasonality remains very similar in all three simulations, consistent with the similar seasonality of the simulated discharges for the Rhine and Rhone rivers (Fig. E2).

#### 4.2.2 Reservoir production

Similarly, a 30-minute time series of observed production by reservoir power plants is prescribed to the model. To fulfill this demand, the model completes first computes the non-dispatchable production that may be available from reservoir spillage and constrained releases, by operating reservoirs according to the rules defined in Sect. 2.3. Figure 11 details how the simulation compares to the prescribed production throughout the period when forced by SAFRAN. Simulated production under the other

forcings is presented in Fig. C3 and C5. Figure 12 displays the co-evolution of the observed national hydraulic stock (RTE, b) and the one simulated in by the model (Eq. (17)) for with the three forcings under study.

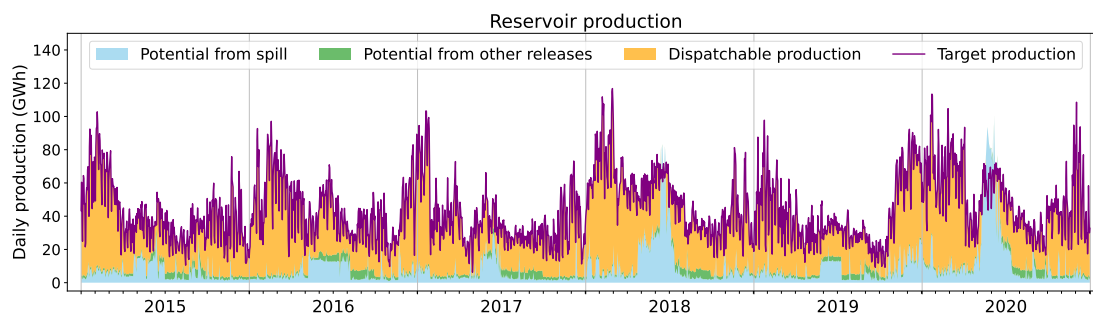


**Figure 11.** National-reservoir-plant-Daily production simulated-in-the-model from reservoir plants. The purple line indicates the production prescribed to the model, while-the-The other colors refer to the nature of the flow that contributes to this-the-simulated production. Blue represents the gross potential from reservoir spillage (water overflowing from the reservoir), green represents the potential from constrained releases of from the reservoirs, and lastly orange represents the dispatchable production, generated by the water that-is specifically released from-the-reservoir for hydropower-purposes power generation.

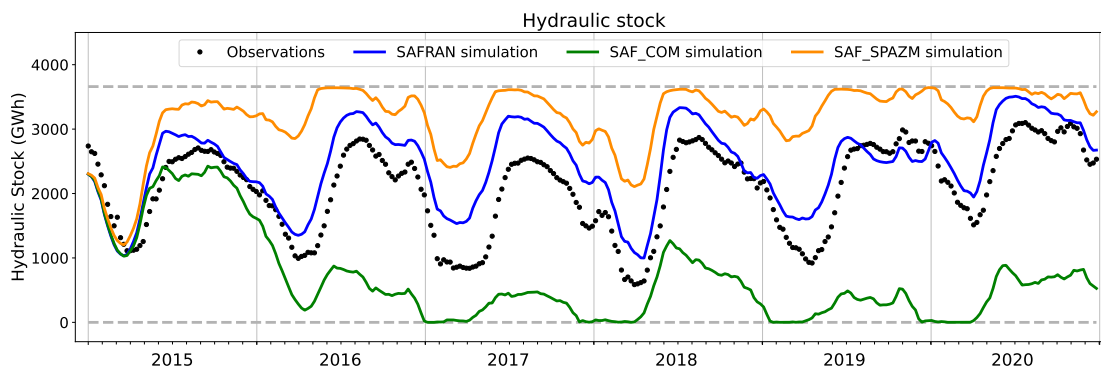


**Figure 12.** Comparison of simulated and observed national hydraulic stock evolution simulated-by-the-model-and-weekly-observations.

Under SAFRAN, the model successfully meets the production target while simulating hydraulic stock variations consistent with observations throughout the six-year period. Reservoirs are filled during the spring due to snow-melt-snowmelt and 505 depleted during the winter to meet the high electricity demand. Nevertheless, a slight temporal shift is observed, as the simulated stock starts to fill some weeks earlier compared to the observations. This temporal shift aligns with the seasonal biases in river discharges identified at the Chamonix Station (Fig. E4), indicating a consistent pattern.



Under SAF\_SPAZM, the stock remains significantly higher than the observations. Indeed, the simulated annual potential of reservoir power plants exceeds their observed production (Fig. 9), resulting in reduced releases from the reservoirs to meet the prescribed demand. This leads to high levels of unused spillage, as shown in Fig. C3.

Under SAF\_COM, however, the stock is completely ~~emptied~~ depleted after the two first years of simulation, and a significant portion of the demand cannot be satisfied (Fig. C5). This is consistent with the huge difference in annual production estimates highlighted in Fig. 9. In addition to the substantial deficit in hydropower potential, a negative feedback loop comes into play. As the reservoir storage diminishes, the head of the power plants decreases, ~~consequently reducing the associated~~ reducing the power generation for a given released volume. Consequently, ~~the power plants draw more water~~ more water is drawn to generate the same amount of energy, further exacerbating the decline in reservoir storage. The calibration carried out relative to SAFRAN is not effective in avoiding this outcome.

Figure 11 allows for the distinction of the different drivers of French hydropower production, depending on the season. In winter, hydropower production is substantial, driven primarily by high electricity ~~consumption~~ The majority of demand. ~~Most~~ of the production stems from intentional reservoir operations, with a minimal ~~proportion~~ portion attributed to fatal production. In spring, fatal production becomes more prominent, particularly due to ~~snow melt-induced~~ snowmelt-induced spillage, resulting in a minimum hourly production, even during periods of low ~~consumption~~ power demand, such as at night (only visible at the hourly resolution not displayed here). During summer, ~~although there is no spillage~~, a significant portion of the hydropower potential comes from constrained ecological and agricultural water releases. When looking at the hourly production (not displayed here), we find a good agreement between the simulated ~~minimal~~ minimum production and the observed troughs in RTE's production.

### 4.3 Effects of hydropower operations on river discharges

We explore in this section ~~to what extent~~ the extent to which the representation of hydropower operations can reduce the hydro-meteorological errors of the model discussed in Appendix E, ~~with~~ using the example of two gauging stations located in the Alps. Figure 13 details the location of these stations comparatively to the hydropower network. The Aigubelle station is located on the Arc river, just upstream of its confluence with the Isère river, and downstream from a series of hydropower plants, including one that generates electricity through the ~~release of~~ releases from a dam on the Isère river. The Cheylas station is located on the Isère river, downstream of its confluence with the Arc.

Figure 14 compares the seasonality of the discharges simulated at these two locations by ORCHIDEE forced by SAFRAN with and without activating the hydropower operations module.

At the Aigubelle station, implementing hydropower operations significantly reduces the annual bias from -31% to -4% (Fig. 14). Indeed, when hydropower operations are activated, a portion of the Isère's water is diverted from its natural outlet to supply a power plant on the Arc. At Cheylas, no change is observed in the bias of the simulated river discharge. Furthermore, the ~~discharge seasonality is improved for both stations~~ seasonality of discharge is improved at both stations, with higher flows in ~~Fall and Winter~~ fall and winter due to releases for power generation. This results in a significant improvement in the NSE metric.

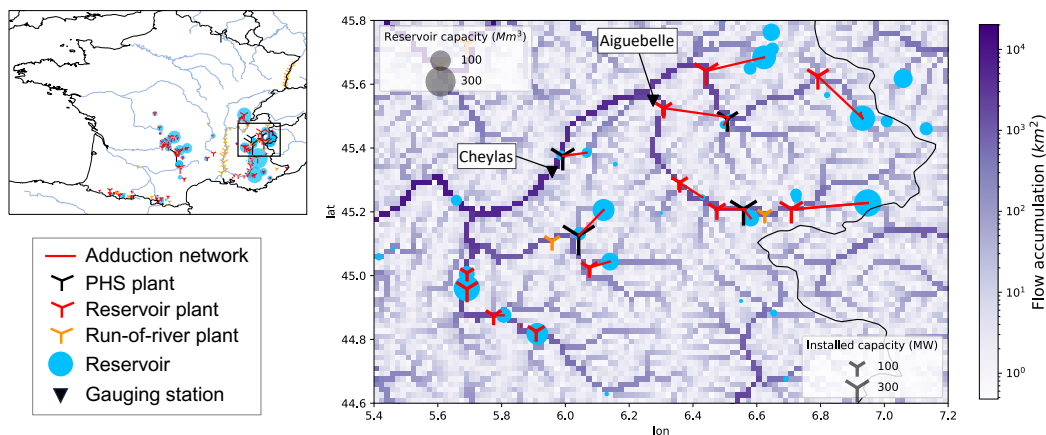


**Figure 13.** Location of Aiguebelle and Cheylas stations comparatively to hydropower infrastructures in Arc catchment (French Alps). PHS plants are pumped-hydro storage plants not considered in this study.

We found a similar effect for other French watersheds where flow observations near hydropower plants are available. However, as mentioned earlier, the [professional-secrecy-confidentiality](#) surrounding French hydroelectric production complicates a systematic and precise evaluation of this improvement in flow simulation.

## 545 5 Discussion and conclusion

### 5.1 A demand-based approach

This study demonstrated the effectiveness of a demand-based approach to simulate hydropower operations in land surface models. The conceptual framework of [such-an-this](#) approach was first described, emphasizing its three original features: (i) the reconstruction of the human-made hydropower network [on-within](#) the model grid to represent not only natural water flows  
550 but also those built for hydropower management; (ii) the implementation of reservoir operation rules that account for their [multi-purpose-objectives; multipurpose objectives; and](#) (iii) the prescription of an exogenous “hydropower demand” defined at the power grid level to drive the release rules of hydroelectric reservoirs, allowing [the](#) coordinated management of all hydroelectric resources on the power grid [and-consistent-in-line](#) with power system needs. Subsequently, we assessed the performance of this approach when implemented in the routing module of the ORCHIDEE model, for the case study of  
555 the French power grid. The ORCHIDEE model was run driven by an atmospheric reanalysis dataset and national historic hydropower production time series were prescribed to the model as the hydropower demand to satisfy. The results indicate that [,](#) when the model is forced to reproduce the historic generation, the implemented method simulates hydroelectric reservoir operations in line with [the](#) observations of reservoir storage at the national level.

Beyond this satisfactory result, our method presents several limitations and opportunities for improvement.

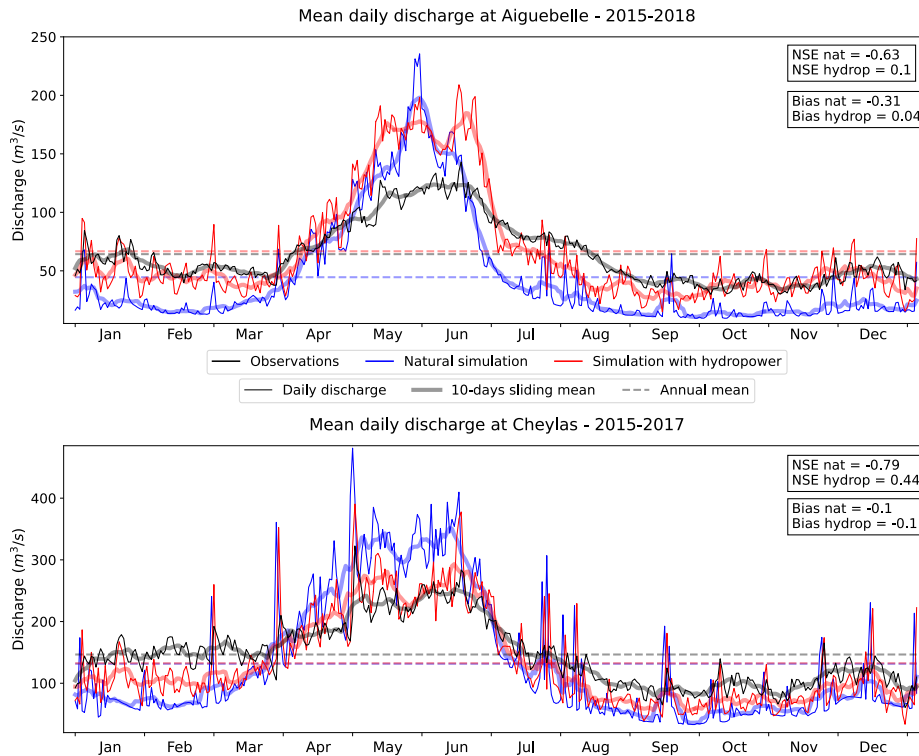


**Figure 14.** Comparison of daily (fine line) simulated river discharge with hydropower operations (red) and without (blue) and observed discharge (black) for two gauging stations in the French Alps. The thicker line is the 10-day average while the dashed line is the annual mean.

560 First, the time series used to drive the reservoir releases in this study is the actual production of dispatchable hydropower plants, which may differ from the real demand for dispatchable hydropower production. Indeed, the actual production is the result of a trade-off between the demand and the prevailing hydrological conditions, particularly the **current** storage level in reservoirs. If this storage is low, the demand **will might** not be fully satisfied **in order to maintain a certain level for future uses to** **preserve water for future needs**. Besides, we consider an exogenous dispatch of the hydropower production across the different

565 types of hydropower plants (namely run-of-river and reservoir) at each time step. This approach facilitates the identification of model deficiencies for each type of power plant. For instance, we found a seasonal bias in **run-of-the-river run-of-river** hydropower production, that would have been overlooked if a single production target had been used for all power plants. The reservoir plants would have served as buffers, reducing their production during periods of excess **run-of-the-river run-of-river** output and increasing it during periods of deficits, thereby resulting in discrepancies in the stock evolution. However, in real-

570 ity, the dispatch of power demand across the different types of hydropower plants is not exogenous but also depends on the hydrological conditions, as the potential for **run-of-the-river run-of-river** production is fully exploited before turning to dispatchable units. To capture these intricate interactions between hydrology and hydropower production decisions, a solution is

to couple our model with an economic power system dispatch model (Oikonomou et al., 2022). This coupling would ensure that the power demand dispatch used to drive reservoir operations in ORCHIDEE considers the hydrological ~~states-conditions~~ simulated within the ~~ORCHIDEE~~-model. This would result in a comprehensive modeling framework wherein simulated hydropower production simultaneously adheres to constraints related to water availability, non-power reservoir operations, and minimization of power system costs. In particular, hydropower demand would be endogenously adjusted to match the hydropower potentials of the simulated hydrology and could avoid entering the feedback loop where reservoirs are emptied, as in the SAF\_COM simulation. This novel approach holds significant promises for enhancing the consistency and realism of hydropower production ~~simulations~~simulations, in particular ~~the study of~~ to study the joint impacts of climate change and variable renewable energy integration.

Second, in this study, we opted for a simple rule to distribute national production among ~~different power plants~~the power plants, and demonstrated that such a rule could simulate credible hydroelectric operations at the national level. ~~As~~ Since no time series of production ~~is available at the individual plant level~~ data is available for individual plants in France, the realism of the simulated ~~individual operations is difficult to assess. This choice can, however,~~ operations at the granular level cannot be assessed. However, the choice of the distribution rule could be further investigated, in particular by testing alternative ~~distribution~~-rules, such as those proposed by Lund and Guzman (1999). Additionally, the operations we simulate assume that a social planner controls the entire grid's power plants and reservoirs, optimizing the collective production. In reality, power plants may belong to different stakeholders, each seeking to maximize their profit. Ambec and Doucet (2003) have shown that such decentralized management can lead to suboptimal resource management, which could not be reproduced by the proposed model. However, in the case of France, our assumption is justified as the historical production company, EDF, owns nearly 85% of the hydroelectric production.

Third, as we focused primarily on hydroelectric usage, other water uses are simplified or even ~~absent~~ omitted in the current version of ~~our~~ the model. Specifically, no water abstraction for domestic, industrial, or ~~agronomie~~ agricultural needs is included ~~in our model~~. Following Zhou et al. (2021), the irrigation demand could be explicitly calculated by the model based on the deficit between potential ~~evaporation~~ and actual evapotranspiration. In other studies, domestic and industrial water demands are estimated using socio-economic proxies such as population density or GDP (Neverre, 2015).

## 5.2 Sources of uncertainties

We have paid particular attention to identifying and discriminating among the various sources of uncertainty that may affect the estimation of hydroelectric production using such a method. Our findings indicate that while errors in simulated discharge are prevalent in most watersheds in our case study, the limited knowledge of the hydroelectric adduction network is the main source of uncertainty for hydropower infrastructures in mountainous basins. To our knowledge, no dataset comprehensively documents these complex "hydroelectric links", which operate on a small scale. Therefore, an in-depth analysis of the gray literature released by the various stakeholders is necessary to reconstruct this network in detail. Furthermore, we proposed a calibration method to overcome this limitation and validated it against observations for the case study of France. This method can therefore be extended to countries with limited information available on the hydroelectric network.

Regarding hydro-meteorological errors, the use of three different precipitation datasets allows us to understand their more precise origin. In several watersheds crucial for hydroelectricity (such as Durance or Lot), and especially in the upstream parts, uncertainties in observed precipitation appear to be the primary contributor to the error in simulated discharge. On the Rhone  
610 or the Rhine rivers, on the contrary, errors in the simulated discharges seem to stem more from processes not represented in the model, such as water withdrawals for human uses, ~~for example~~. Though incomplete, this work contributes to the current effort to integrate human water management into hydrological models, in order to simulate a more realistic water cycle (Nazemi and Wheater, 2015a). We show that our method can improve river flow simulations in some mountain catchments where hydropower cannot be neglected.

615 Finally, our study shows that comparing hydropower estimates with observed production offers an indirect means of ~~checking~~ assessing the quality of ~~meteorologic~~ meteorological data. In our study case, we ~~demonstrate~~ demonstrated the lower quality of the COMEPHORE dataset in mountainous regions compared to SAFRAN or SPAZM, something already identified by Birman et al. (2017); Magand et al. (2018).

### 5.3 Perspectives

620 In conclusion, the demand-based operations proposed in this study hold promising prospects for enhancing our understanding of the resilience of different power mix scenarios to changes in climate, water management, or land use. The next steps in this trajectory involve (i) integrating our climate-based hydropower model with a power system model to get a comprehensive framework that captures all relevant constraints on hydropower production, (ii) applying this integrated framework to climate change scenarios and power system scenarios to ~~assess~~ evaluate the adaptive capacity of the power grids, and (iii) refining the  
625 description of other water uses to more completely describe the competition for water resources.

Such a detailed model could also be instrumental in planning future hydropower expansion more sustainably. It would help assess the demand satisfied by new hydropower plants at the grid scale, considering both existing and planned hydropower plants. Besides, the model could evaluate the potential impacts of new projects on river discharges and ecosystems.

*Code and data availability.* The ORCHIDEE version developed for this project is available upon request. The meteorological forcings used  
630 in this study were provided by Meteo-France for SAFRAN (<https://www.umr-cnrm.fr/spip.php?article788&lang=en>) and COMEPHORE (<https://radarsmf.aeris-data.fr/en/home-page/>), and EDF-DTG for SPAZM (Gottardi et al., 2008)). The observed data used for validation is openly accessible online. River discharge data can be downloaded at <https://hydro.eaufrance.fr/>, while data on energy production is available at <https://opendata.reseaux-energies.fr/>. The reservoir dataset was built based on the GRanD database (Lehner et al., 2011), which can be found at <https://www.globaldamwatch.org/grand/>, and on the data of the *Comité Français des Barrages et Réservoirs* (CFBR) at <https://www.barrages-cfbr.eu/-En-France->. Finally, the plant's database was built from the EU JRC hydro-power plants database (<https://github.com/energy-modelling-toolkit/hydro-power-database>) and the *Registre national des installations de production raccordées au réseau de transport d'électricité*, which can be downloaded at <https://opendata.reseaux-energies.fr/>.

## Appendix A: Building the routing network

### A1 Locating hydroelectric infrastructures on the river network

640 Dams and hydropower plants are located on the MERIT grid based on ~~geo-referenced~~ georeferenced and upstream area information provided in the databases (~~Infrastructures~~. The infrastructure datasets used for our study over France the France case study are presented in Appendix B). The location procedure is done following these steps:

1. ~~We identify a first location based on the infrastructure's~~ The initial location is identified based on geographical coordinates.
- 645 2. ~~We define a search area around this first~~ A search area is defined around this initial location (typically with a 10km in radius)
  - If the upstream area of the infrastructure is ~~informed~~ available in the databases, we identify all the pixels in the search area ~~having that have~~ an upstream area close enough to the one being searched to the referenced one (typically +/- 20%) ~~and, among~~. Among these eligible pixels, the one closest to the first initial location is selected. If no  
650 pixel ~~checks this condition~~ meets the criteria, the infrastructure is not placed.
  - ~~Otherwise~~ If no upstream area data is available in the databases, we look for the closest pixel to the first location initial location that is likely to be ~~positioned~~ situated on a river. To do this, the maximum upstream area of the pixels in the search area is identified ( $U_{max}$ ) and the closest pixel to the first guess pixel satisfying (initial location satisfying the condition  $U > \frac{U_{max}}{10}$  ) is selected, with where  $U$  being is the upstream area of the pixel.

655 Note that each vertex and edge can respectively contain only one dam ~~or and~~ hydropower plant. If several reservoirs dams are placed on the same HTU during pixel aggregation, their respective reservoir volumes for the different uses are summed. If two plants are placed on the same edge, their installed power ~~and pumping capacity as well as their~~ capacity and head are summed only if both plants have the same input point. Otherwise, only the plant with the highest installed capacity is kept. As in other studies (Abeshu et al., 2023), all the reservoir attributes are associated with the HTU of the dam (even if its water  
660 surface can be larger than the HTU area and its geometry is different from the HTU geometry).

### A2 Adduction network

Poundage and reservoir plants generate electricity from the water released from ~~the~~ upper reservoirs. To explicitly represent this adduction network in our model, we ~~have~~ need to identify such connections between a feeding reservoir and a power plant. Since datasets describing these connections are rarely available, we use an algorithm to identify ~~these connections~~ them.  
665 For each poundage or reservoir plant, we ~~thus~~ select as the feeding reservoir the one that maximizes the potential function  $\phi = \frac{U * V * h}{d}$ , where  $U$  is the upstream area of the dam,  $V$  is the storage capacity of the reservoir,  $h$  is the elevation difference between the plant and the reservoir dam and  $d$  is the horizontal distance between them. The definition of ~~these potential~~

~~functions~~ this potential function is inspired by similar ~~works~~ approaches aiming to connect an irrigated area to a water supply point (Neverre, 2015; Zhou et al., 2021).

670 This position algorithm relies on the assumption that each plant is fed by only one reservoir. This assumption is however debatable, especially for plants in ~~mountain areas that~~ mountainous regions, which may be connected to several reservoirs. In this case, ~~our choice of~~ the potential function  $\phi$  privileges the reservoir with the largest upstream area ~~since~~, as it is likely to ~~determine the production potential of the plants~~ have the most significant influence on the plant's production potential. During calibration (see Sect. 2.5), plants for which the identification of a single reservoir conducts to a significant misrepresentation  
675 of the plant's ~~hydropower~~ production potential are identified and a correction is made by moving the withdrawal point so that it gathers enough water to ensure the observed production is possible.

## Appendix B: Datasets

### B1 Dams and reservoirs

We use global reservoir data from GRanD (Global Reservoirs and Dams) dataset (Lehner et al., 2011), which gathers data of  
680 compiles data on large reservoirs and dams worldwide (volume  $> 0.1 km^3$ , hence a total of totaling 7320 dams). The database  
contains includes 137 dams in France, 63 of which are used for hydroelectricity. However, some important dams for French  
hydroelectricity are not documented in this database. Therefore we completed the database for this study dataset with data  
from the CFBR (Comité Français des Barrages et des Réservoirs), which is in charge of responsible for the inventory of French  
dams higher than 15m for the ICOLD (International Commission on Large Dams). We extracted data from its website (CFBR,  
685 2021) to complete the GRanD database. Our database finally gathers final dataset comprises 492 French dams. Their location,  
original database data sources, and intended purposes are shown in Fig. B1.

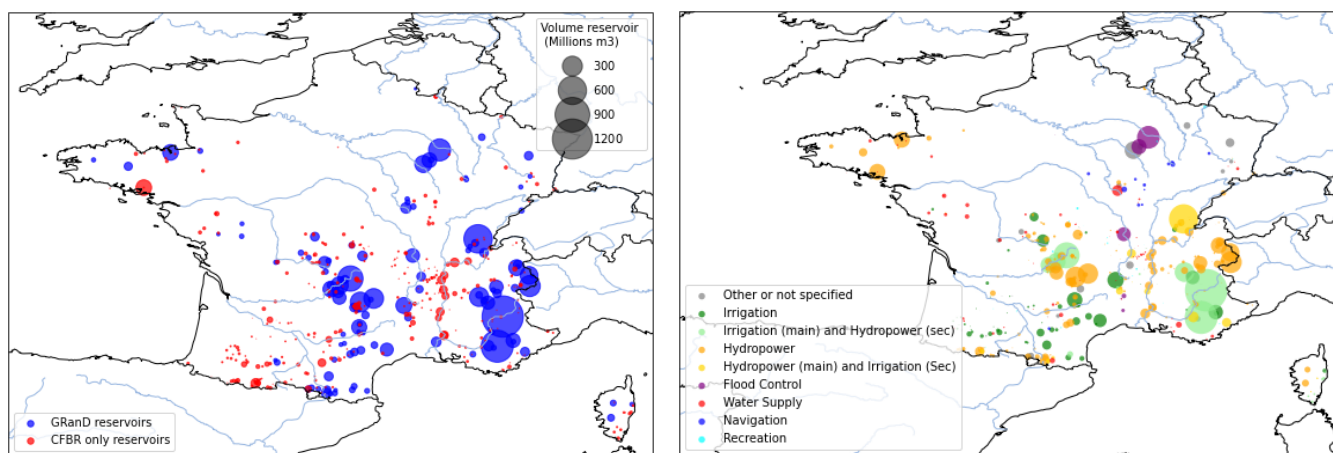


**Figure B1.** Location and main uses of the reservoirs in the final database

### B2 Hydropower plants

The data used in this study are obtained from the EU Joint Research Center Hydro-power plants database (European Commission and Joint F  
European Commission and Joint Research Centre (JRC) (2019) database. This database gathers includes geographical coord-  
690 inates, installed power capacity, plant type (run-of-river, reservoir, or pumped-hydro storage (PHS)), and hydraulic head  
information for 4186 European plants (for a total, totaling an installed capacity of 161 GW). Of these, 153 of these plants are  
located in France, representing 20.6 GW of capacity. Other available datasets of French hydropower plants are the national  
registers of electricity generation and storage facilities published annually (ODRÉ, 2016, 2018). The 2016 register gathers  
data from includes data on 414 hydropower plants, with a total installed capacity of 23.4 GW. However, as these registers do  
695 not provide the geographical coordinates of the plants, we chose to use the JRC database. Nevertheless, we use data from the  
2016 national register to rectify correct head information and categorize the plants in according to the 4 categories used by the



French operator: run-of-river, poundage, reservoir, and PHS. Figure B2 shows the locations of the plants included in our final database, while Table B1 summarizes the discrepancies between the databases in terms of installed capacities.

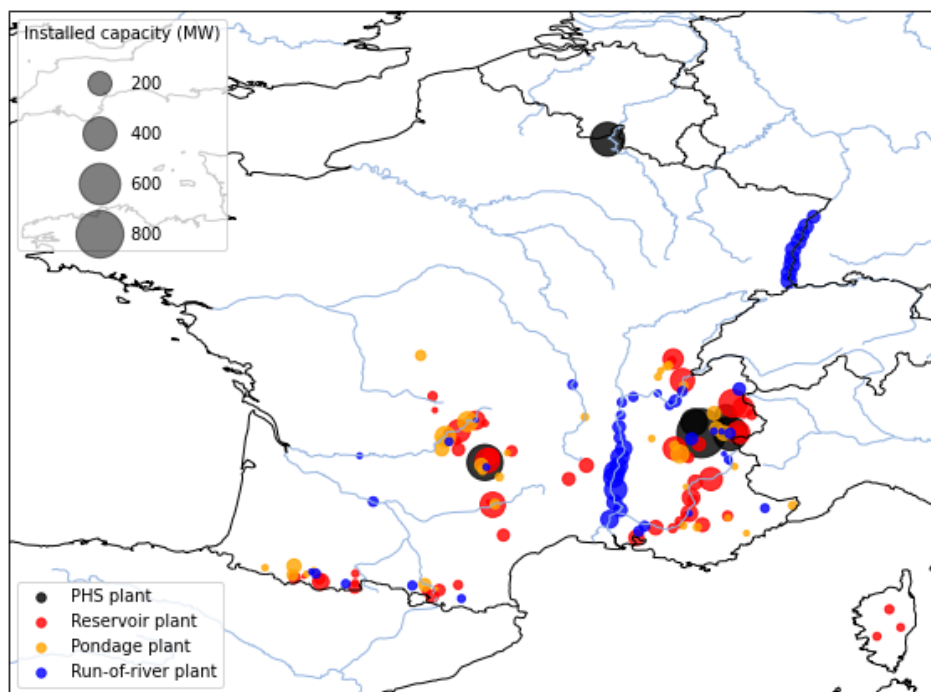


**Figure B2.** Typology of the plants in the database

	Total	Run-of-river	Poundage	Reservoir
National Register 2016 (ODRÉ, 2016)	23.426	5.943	3.715	8.748
JRC (initial categories)	19.695	5.87	-	8.76
Final database (plants from JRC database, classified following RTE categories which have been located on HTUs)	19.638	4.426	2.606	7.434
<i>compared to ODRÉ (2016)</i>	<i>84.6%</i>	<i>74.2%</i>	<i>71.7%</i>	<i>86.0%</i>

**Table B1.** Comparison of the different databases in terms of installed hydroelectric capacities (GW) in metropolitan France (without Corse et DOM-TOM)

### B3 Conversion factors for hydropower generation

700 As presented in Table B1, our final dataset does not include all the hydropower plants installed in France. However, by using annual production data of each plant provided by ODRÉ (2015, 2016, 2018), we can quantify-estimate the share of the national

production ~~provided by the power plants~~ accounted by the plants included in our database. This ~~enables~~ allows us to compute a factor to convert the actual production of national time-series (RTE, a) into representative production in our model, both for prescribing the production demand and comparing the results. The computation of such conversion factors is presented in Table B2. It relies on the assumption that within each category of power plant, the geographical distribution of plants in our database is representative of all French power plants so that production ratios remain constant over time. This assumption is debatable as our database primarily includes the largest power plants in terms of installed capacity, which are predominantly often concentrated in certain regions, while ~~smaller-scale~~ smaller plants may be located in watersheds not represented in our database (e.g., run-of-river plants on the ~~River Seine~~ Seine river for instance). However, as the missing plants have, by definition, a lower installed capacity than those in our database, their contribution to national production is lower and can reasonably be neglected.

	Total	Run-of-river	Poundage	Reservoir
National production in 2016 (RTE et al., 2016)	62.6	31.6	9.4	15.8
Total production from plants in national register in 2016 (ODRÉ, 2016)	57.6	27.5	9.0	15.6
<i>compared to RTE et al. (2016)</i>	<i>92.0%</i>	<i>87.0%</i>	<i>95.7</i>	<i>98.7%</i>
Total production from plants in the database in 2016 (based on ODRÉ (2016))	47.9	22.4	5.5	14.1
Coefficients 2016		70.9%	58.5%	89.3%
<hr/>				
National production in 2018 (RTE et al., 2018)	66.9	31.3	10.9	18.8
Total production from plants in national register in 2018 (ODRÉ, 2018)	60.7	26.4	10.0	18.3
<i>compared to RTE et al. (2018)</i>	<i>90.7%</i>	<i>84.3%</i>	<i>91.7%</i>	<i>97.3%</i>
Total production from plants in the database in 2016 (based on ODRÉ (2018))	48.1	20.5	6.0	16.2
Coefficients 2018		65.5%	55.0%	86.1%
<hr/>				
<b>Conversion factors</b>		<b>68.2%</b>	<b>56.8%</b>	<b>87.7%</b>

**Table B2.** Comparison of the different available databases in terms of annual production (TWh) and calculation of conversion factors.  
n.a.=not available

## Appendix C: Alternative precipitation datasets

### C1 ~~Presentation of the datasets~~ Datasets presentation

#### C1.1 COMEPHORE

715 COMEPHORE (COMbinaison en vue de la Meilleure Estimation de la Précipitation HOraiRE) dataset provides observations  
of surface precipitation accumulation over metropolitan France at an hourly and kilometeric resolution based on a synthesis of  
radar and rain gauge data. A specific processing chain has been implemented in order to address the various sources of error  
affecting radar data, in particular its low quality in high altitude mountainous areas like the Alps or the Pyrenees (Fumière  
et al., 2020). The final database is nevertheless assumed to be the best representation of surface precipitation over metropolitan  
720 France (Fumière et al., 2020).

We build a meteorologic dataset SAF\_COM by replacing precipitation data in SAFRAN with data from COMEPHORE. As  
COMEPHORE does not distinguish solid and liquid precipitations, we keep SAFRAN's hourly ratio of solid/liquid precipita-  
tions when possible and discriminate based on the air temperature otherwise.

The differences in annual mean precipitation ~~are generally small~~ between SAFRAN and COMEPHORE are generally small,  
725 with an average deviation inferior to 1.0% ~~in COMEPHORE compared to SAFRAN~~ (Fig. C1). However, we find a small  
seasonal bias as this average deviation goes ranges from -2.0% ~~for the Winter period in winter~~ to +1.9% in the Summersummer.  
Moreover, discrepancies increase dramatically in mountainous regions, especially in the Alps and the Pyrenees. For grid points  
with an average elevation above 1000m, the annual mean precipitation in COMEPHORE is, on average, 10.4% lower than in  
SAFRAN.

#### 730 C1.2 SPAZM

SPAZM (SPAtialisation des précipitations en Zone de Montagne) is a daily reanalysis of precipitation at the kilometer scale,  
developed by EDF, ~~the France's~~ the France's main electricity producer ~~in France~~. SPAZM specifically covers the southern half of the French  
territory, where a large majority of hydroelectric power plants are located (Gottardi et al., 2008). Climatological precipitation  
outlines are first constructed based on daily precipitation observations categorized by types of oceanic circulation (weather pat-  
735 terns) ~~(Garavaglia et al., 2011)~~. These outlines are then spatially interpolated onto the kilometer-scale grid and deformed daily  
according to available observations. In addition to Météo-France's observations, which are also used to construct SAFRAN,  
EDF's measurement network is utilized. We interpolate the daily precipitation data from SPAZM to the hourly scale and merge  
it with SAFRAN data to create the alternative forcing dataset SAF\_SPAZM. As for SAF\_COM, we keep SAFRAN's hourly  
ratio of solid/liquid precipitations when possible. Compared to SAFRAN, ~~precipitations are in SPAZM's precipitations are~~  
740 on average 2.7% higher in SPAZM with an average bias of, with a bias of +7.0% in Summer, against summer and +2.1% in  
Winter. Bias winter. The bias is heterogeneously spread over France (Fig. C1) with bigger larger differences on the highest  
reliefs, without a clear sign ~~(. For grid points above 1000m, the average deviation of +3.9% for grid points above 1000m)~~.

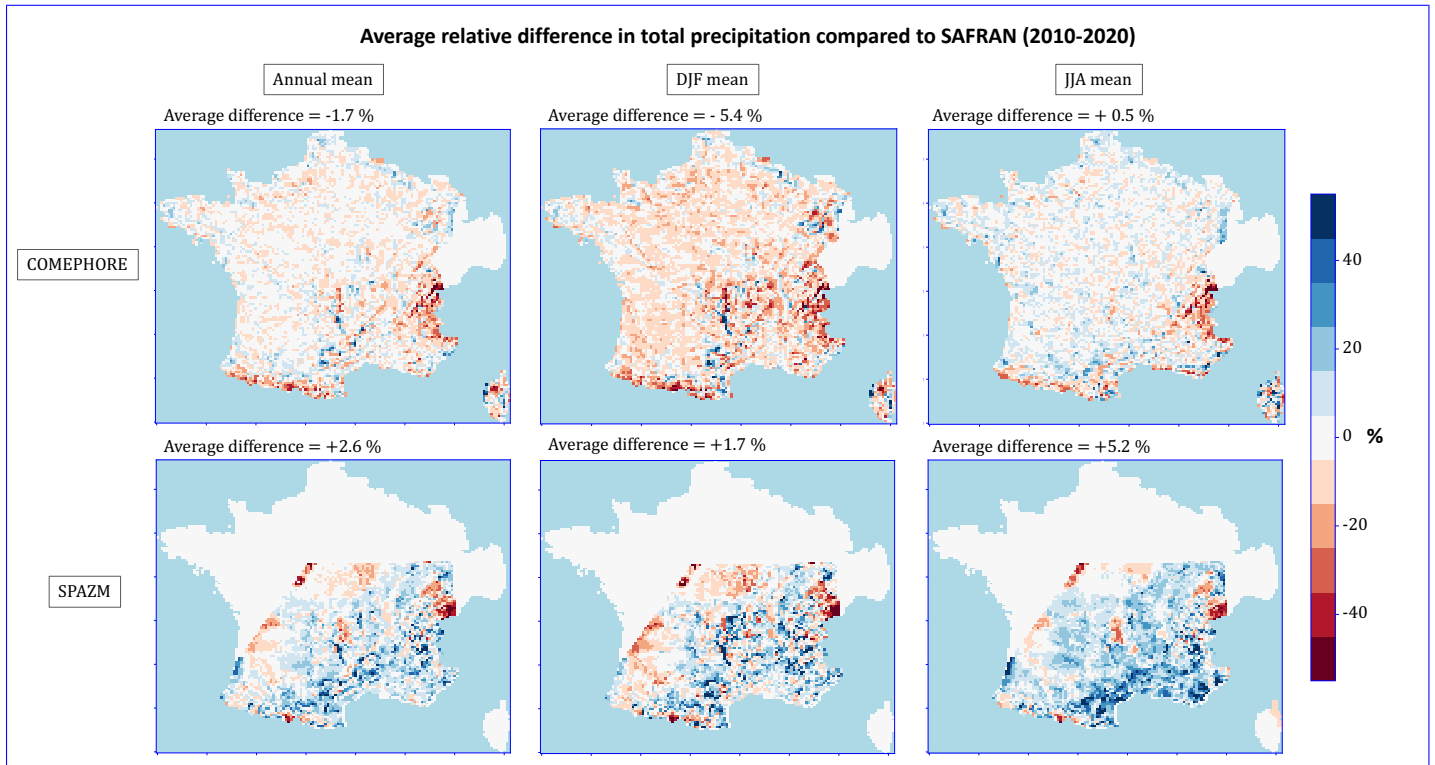


**Figure C1.** Average relative differences in total precipitation across the datasets for the period 2010-2020.

Left column: annual average bias difference, middle: average bias difference in Winter period (December-January-February), right: average difference in Summer period (June-July-August). Top: COMEPHORE dataset compared to SAFRAN, Bottom: SPAZM compared to SAFRAN

**C2 Simulation of hydropower production under SAF\_SPAZM**

**C3 Simulation of hydropower production under SAF\_COM**

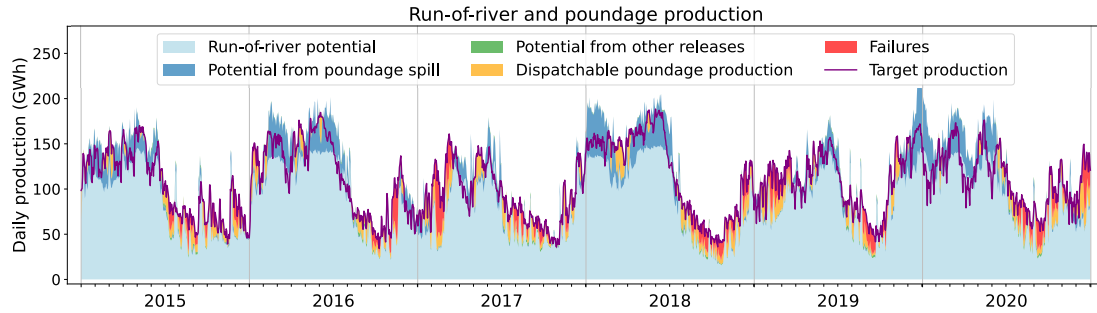


**Figure C2.** National run-of-river plant Daily production from run-of-river and poundage plants simulated in the model when forced by SAF\_SPAZM. The purple line indicates the production that has been prescribed to the model and the red coloring shows the difference between this production and failures of the one simulated in the model when forced by SAF\_SPAZM to meet this target production. The other colors refer to the nature of the flow that contributes to the simulated production in the model. Light blue represents the gross potential of run-of-river plants, dark blue represents the potential of spill from spillage from poundage reservoir reservoirs (water overflowing from the reservoir), green represents the potential from constrained releases of poundage reservoirs, and lastly orange represents the dispatchable production, generated by the water specifically released from the poundage reservoirs for power generation.

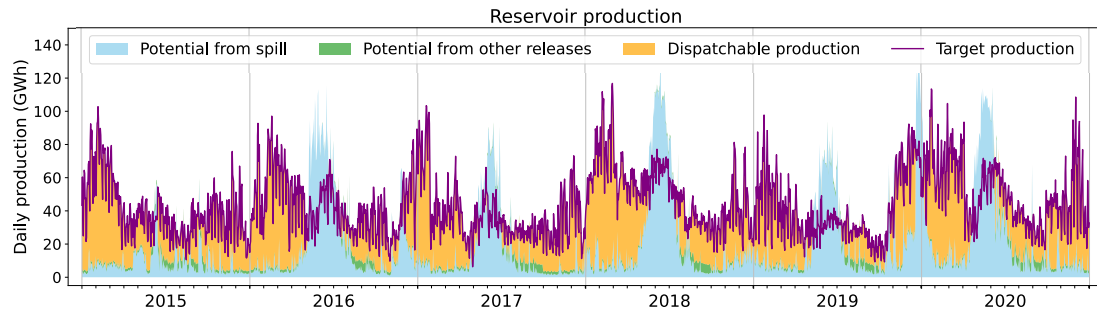


**Figure C3.** National reservoir plant Daily production from reservoir plants simulated in the model when forced by SAF\_SPAZM. The purple line indicates the production that has been prescribed to the model. The other colors refer to the nature of the flow that contributes to this the simulated production. Blue represents the gross potential from reservoir spill spillage (water overflowing from the reservoir), green represents the potential from constrained releases of from the reservoirs, and lastly orange represents the dispatchable production, generated by the water that is specifically released from the reservoir for hydropower purposes power generation.

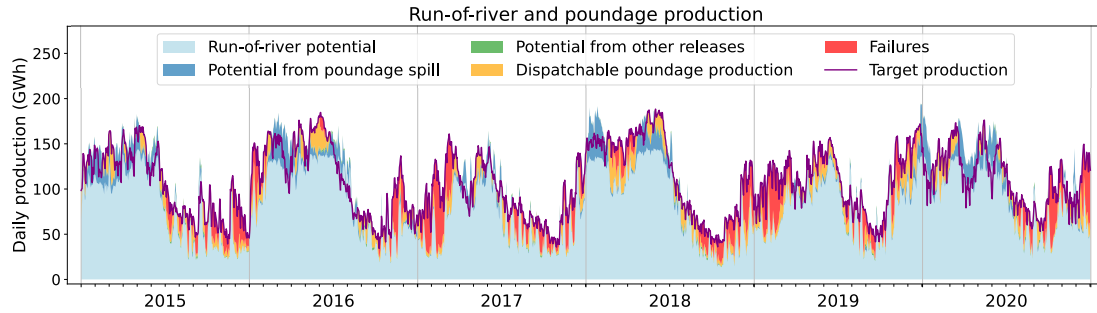


**Figure C4.** National run-of-river plant Daily production from run-of-river and poundage plants simulated in the model when forced by SAF\_COM. The purple line indicates the production that has been prescribed to the model and the red coloring shows the difference between this production and failures of the one simulated in the model when forced by SAF\_COM to meet this target production. The other colors refer to the nature of the flow that contributes to the simulated production in the model. Light blue represents the gross potential of run-of-river plants, dark blue represents the potential of spill from spillage from poundage reservoir reservoirs (water overflowing from the reservoir), green represents the potential from constrained releases of poundage reservoirs, and lastly orange represents the dispatchable production, generated by the water specifically released from the poundage reservoirs for power generation.

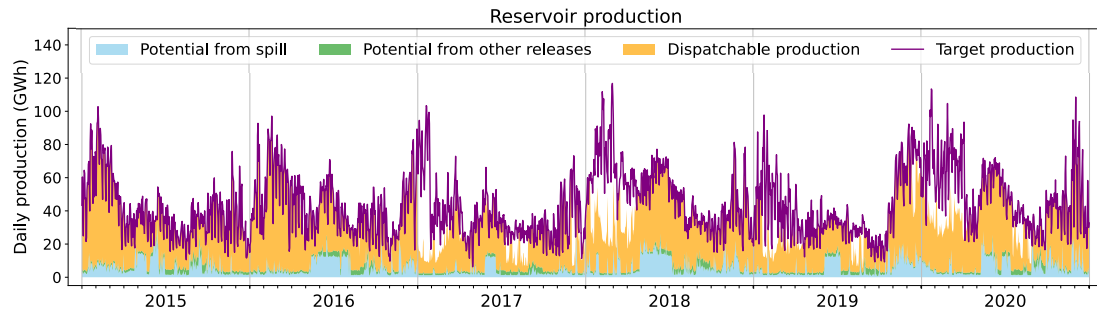


**Figure C5.** National reservoir plant Daily production from reservoir plants simulated in the model when forced by SAF\_COM. The purple line indicates the production that has been prescribed to the model. The other colors refer to the nature of the flow that contributes to this the simulated production. Blue represents the gross potential from reservoir spill spillage (water overflowing from the reservoir), green represents the potential from constrained releases of from the reservoirs, and lastly orange represents the dispatchable production, generated by the water that is specifically released from the reservoir for hydropower purpose power generation.

## 745 Appendix D: Hydropower network error

The La Bathie power plant is the most important reservoir hydropower plant in France in terms of installed ~~capacities~~<sup>capacity</sup>. It is located in the Alps and is fed by numerous water intakes, as illustrated in Fig. D1. ~~Among them, are~~ These include the reservoirs of Roselend, Saint Guérin, and La Gittaz, as well as other intakes directly connected to rivers or glaciers.

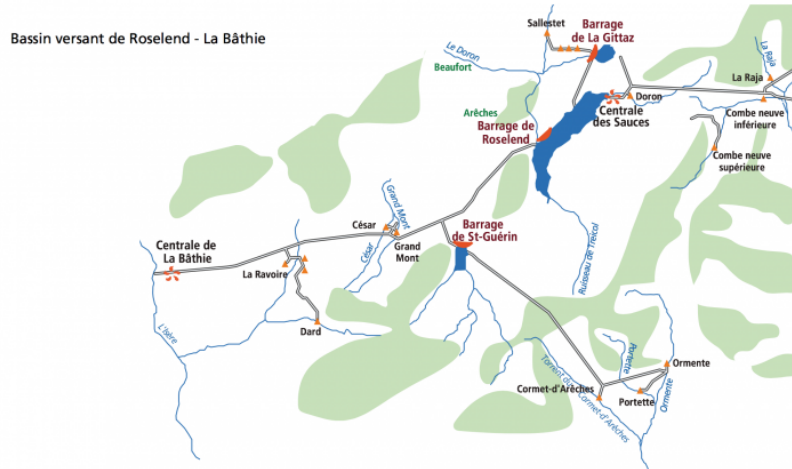


**Figure D1.** Schematic representation of the water aduction network to La Bathie power plant (source:vpah-auvergne-rhone-alpes.fr)

Figure D2 describes the same area in HTUs space and shows that the Roselend reservoir accounts for only a small part of the water being transferred to the hydropower plant.

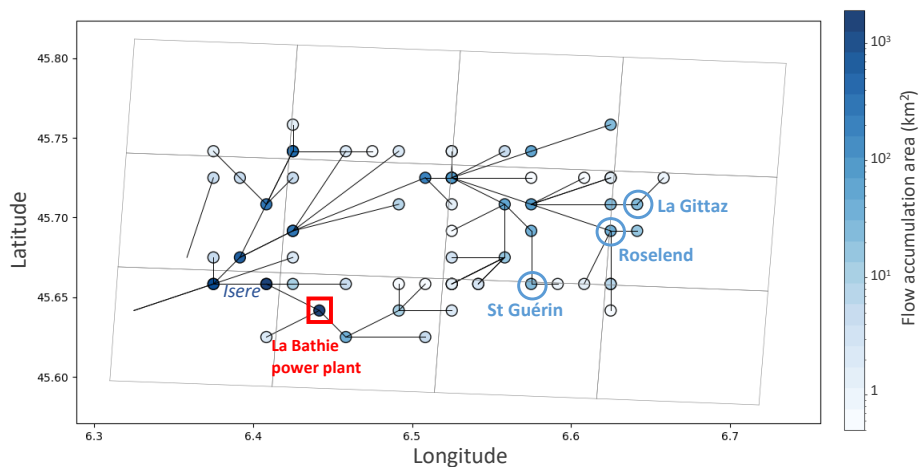


**Figure D2.** HTUs representation in the model for the same spatial area as Figure D1. The location of hydropower infrastructures is indicated.

## Appendix E: Hydro-meteorological errors

To evaluate the performance of the ORCHIDEE model ~~to simulate in~~ simulating river discharges in France, independent of reservoir operations, we compare the daily river discharges simulated by the model with ~~the observations database of Schapi (2022)~~ observations from Schapi (2022) database. It is important to ~~acknowledge~~ note that the observed discharge data  
755 represents actual discharge values, including water withdrawals, while, at this stage, ~~our model~~ ORCHIDEE generates natural discharges without accounting for such withdrawals and dam operations.

### E1 Bias in average discharge

Figure E1 displays ~~relative biases of average~~ the relative biases in the mean discharge simulated by ORCHIDEE forced by SAFRAN over the 2010-2020 period for a selection of gauging stations located on rivers ~~equipped~~ with hydropower infrastruc-  
760 ture (see Fig. B2 for the detailed locations of the power plants). We chose the bias metric because the annual mean discharge is the most relevant parameter for hydropower potential.



Relative bias of mean river discharge simulated by ORCHIDEE forced by SAFRAN over 2010-2020 period

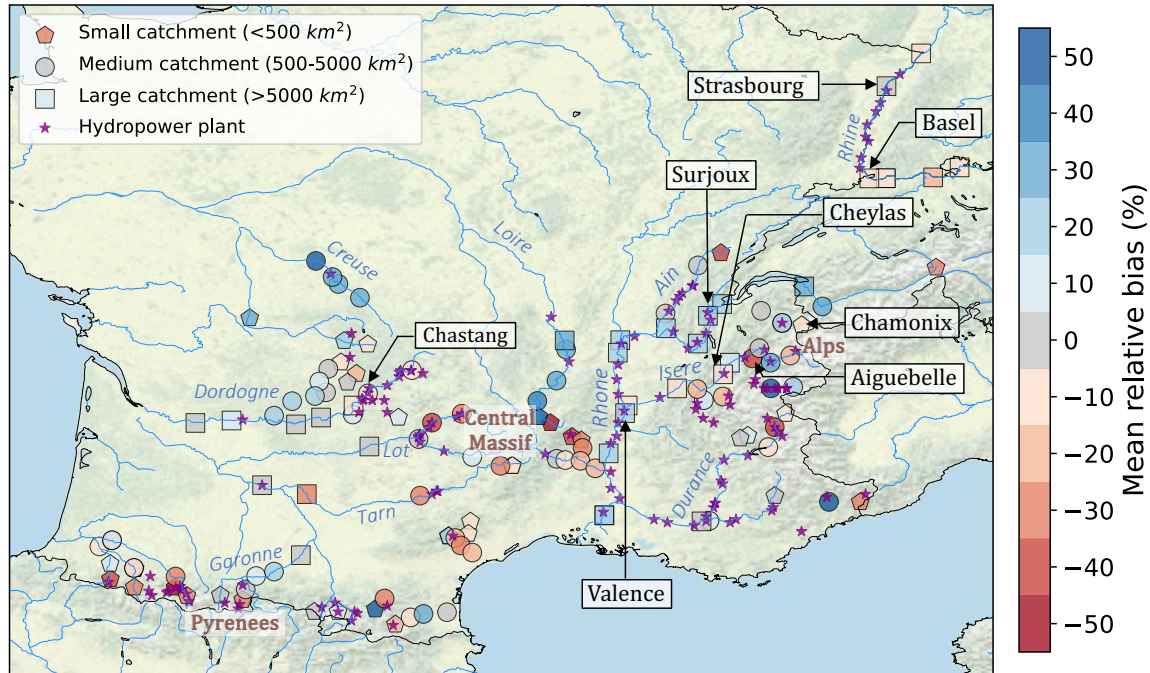


**Figure E1.** Relative bias of average in mean discharge for a selection of gauging stations located on French rivers equipped for hydropower, for the period 2010-2020. Each colored point represents a gauging station, The with the shape indicates indicating the size of the concerned watershed its catchment, while the color indicates the calculated discharge bias at this location. Purple stars indicate the locations of the hydropower plants located on the model grid.

Source: authors Authors, based on a layer by U.S. National Park Service

The overall performance of the model indicates a slight overestimation of flows, with an average bias of +2.4%.

The discharge bias shows an increasing trend increases with the upstream area of stations. For small catchments (less than  $500 \text{ km}^2$ ), the average bias is -1.6%. In medium-sized catchments (between 500 and  $5000 \text{ km}^2$ ), the bias decreases to is +1.1%. In large catchments (more than  $5000 \text{ km}^2$ ), the bias becomes more pronounced, reaching +7.6%. It is however, however, important to note that the smaller the upstream area, the greater the uncertainty in the location of the station. In Fig. E1, only the stations located with an error in the upstream area lower than 20% are displayed.

On the largest rivers (Rhine and Rhone), where most run-of-river power plants are located, the bias shows little spatial variability, constant at remaining around +20% for the Rhone and -10% for the Rhine respectively. In. In contrast, in the Alps, on the other hand, where a significant proportion share of dispatchable hydroelectric capacity is installed, the bias displays a high spatial heterogeneity, sometimes is highly variable, even within the same river. Upstream For instance, upstream of

Iserre river, the bias varies from -19% to +26% between two stations ~~some-located about~~ twenty kilometers apart. The upstream reaches of the Durance also show negative biases.

In the other massifs equipped for hydroelectricity (~~such as~~ the Pyrenees and Massif Central), there are ~~also~~ negative biases at ~~altitude~~ higher altitudes, which gradually diminish downstream.

Assuming negligible observational errors, discharge bias can originate from ~~different~~ several error sources:

- Errors in the atmospheric forcing applied to ORCHIDEE;
- Modeling errors in the ~~representation of~~ energy, water, and carbon cycles;
- Missing processes in ORCHIDEE ~~like, such as~~ glacier melting, interactions with groundwater, and water withdrawals).

To explore the first hypothesis, Fig. E2 compares ~~the~~ discharges simulated by ORCHIDEE using the two alternative forcings (SAF\_COM and SAF\_SPAZM) with ~~those from~~ the reference SAFRAN simulation. The relative biases of these simulations ~~compared~~ to observations are presented in Fig. E3.

Under ~~the~~ SAF\_COM forcing, simulated discharges show relatively small differences ~~on~~ from those obtained with SAFRAN ~~on an~~ annual average, except in mountainous watersheds (Alps and Pyrenees), ~~where~~. ~~In these regions~~, the lower precipitation in ~~COMEPHORE-SAF\_COM~~ results in streamflows that are 30% to 40% lower when compared to the SAFRAN simulation. ~~However~~ ~~Besides~~, a pronounced seasonal pattern is observed. The simulated streamflows ~~in winter~~ are lower in ~~the simulation forced by COMEPHORE winter under SAF\_COM~~ across France (averaging -16% and up to -50% for the Loire and Durance rivers), while ~~in summer~~, they are higher ~~in summer~~ (averaging +25% and up to +50% for the Loire River). ~~As regards~~ ~~Regarding the~~ comparison with observed flows (Fig. E3, the negative biases ~~existing under SAFRAN observed with SAFRAN~~ in the Alps and Pyrenees are accentuated ~~under SAF\_COM~~, particularly along the Durance and Iserre rivers, ~~where~~ many hydroelectric power plants are located. However, for some Alpine stations and the Massif Central, ~~for which~~ ~~where~~ the flow is overestimated with SAFRAN, the flow is more accurately simulated ~~with COMEPHORE under SAF\_COM~~.

Under the SAF\_SPAZM forcing, ~~river discharges show an increase in the majority of watersheds, which is~~ ~~mean river discharges generally increase in most watersheds compared to the SAFRAN simulation~~, consistent with the ~~previously highlighted~~ higher precipitation in this dataset. However, the upper Rhone watershed stands out with a decrease in simulated discharge, reaching up to -40% during the summer season, allowing for a reduction in the bias ~~of simulated discharges in simulated discharge~~ in this area.

~~Even~~ ~~This analysis shows that variability in forcing data significantly influences simulated discharges, even~~ if we limit our analysis to the precipitation variable without considering other forcing variables, ~~we show a significant influence of the forcing variability on the simulated discharges~~.

## E2 Discharge seasonality

Beyond the bias in ~~average mean~~ values, the performance of ORCHIDEE in reproducing the seasonality of the discharge is key for the modeling of run-of-river production as well as that of poundage power plants, which have ~~only a~~ very limited storage

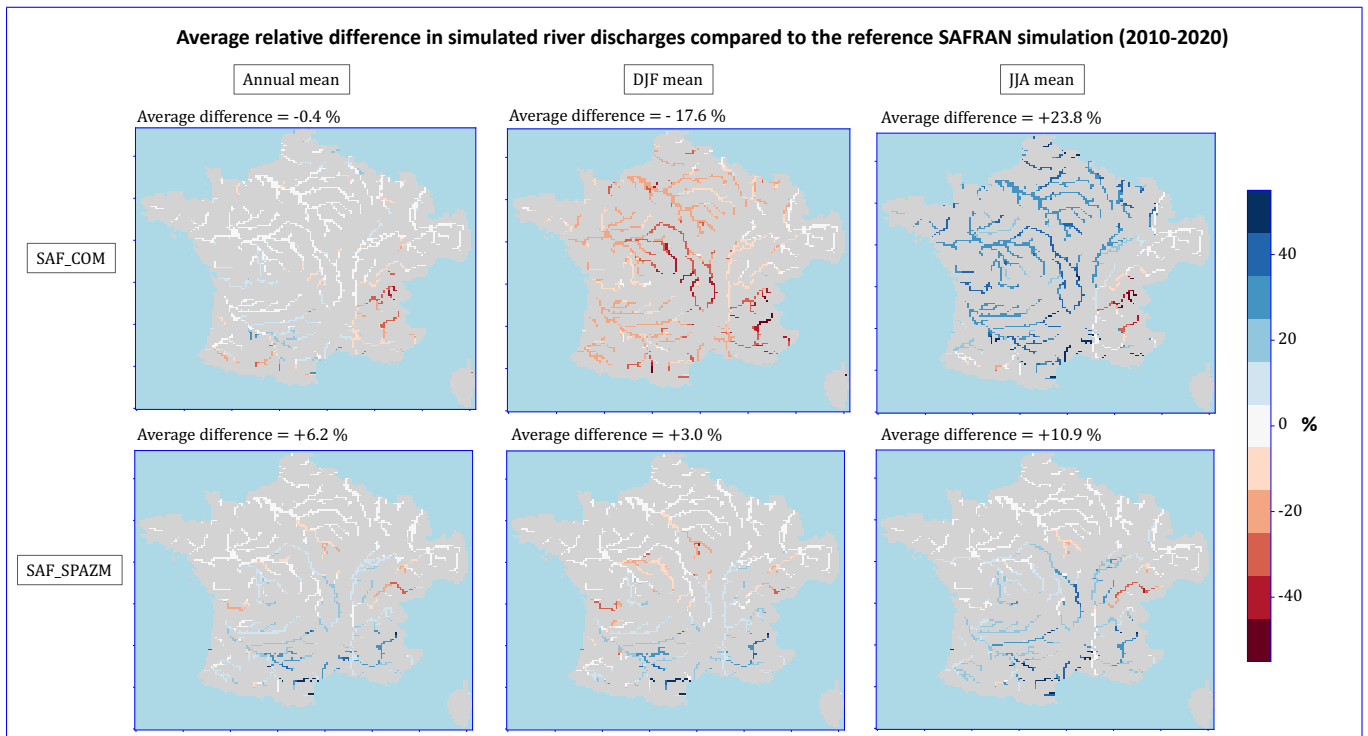


**Figure E2.** Average relative bias-Relative difference in discharge simulated by ORCHIDEE under the alternative precipitation forcings. Results are given in expressed as average relative difference-differences compared to the reference SAFRAN simulation for the period 2010-2020. Left: annual average bias, difference; middle: average bias-difference in the Winter period-winter (December-January-February); right: average difference in the Summer period-summer (June-July-August). The discharges are displayed-shown for all grid points with an upstream area higher-greater than  $1000 \text{ km}^2$ .

capacity. Observations and simulations of daily discharges under the SAFRAN forcing are presented in Fig. E4 for selected gauging stations in catchments equipped with run-of-river or poundage power plants.

As depicted in Fig. B2, run-of-river plants are mostly located along the Rhone and Rhine rivers. In the upper Rhone (Surjoux station), there is a substantial overestimation of high flows and an underestimation of low flows. The error reduces progressively downstream: the Nash Sutcliffe efficiency (NSE) is better at the Valence station, despite a higher overall annual bias (likely due to the non-representation of water withdrawals). On the Rhine (Basel and Strasbourg stations), we see similar errors, with an underestimation of low flows during the Fall and an underestimation of the Spring maximum. The discrepancy in the Rhone's seasonality can be attributed to the non-representation of Lemans reservoir management in our model, which is known to play a crucial role in shaping discharge seasonality in the upper Rhone (Habets et al., 1999).

Poundage plants are distributed across various catchments. Some of them are concentrated in the upper Dordogne river, notably the Chastang plant, the most powerful poundage facility, which benefits from a gauging station at its location. We find a positive NSE for this station, indicating that the seasonality is well captured by the model.

## Relative bias of mean river discharge simulated by ORCHIDEE forced by alternative forcings over 2010-2020 period

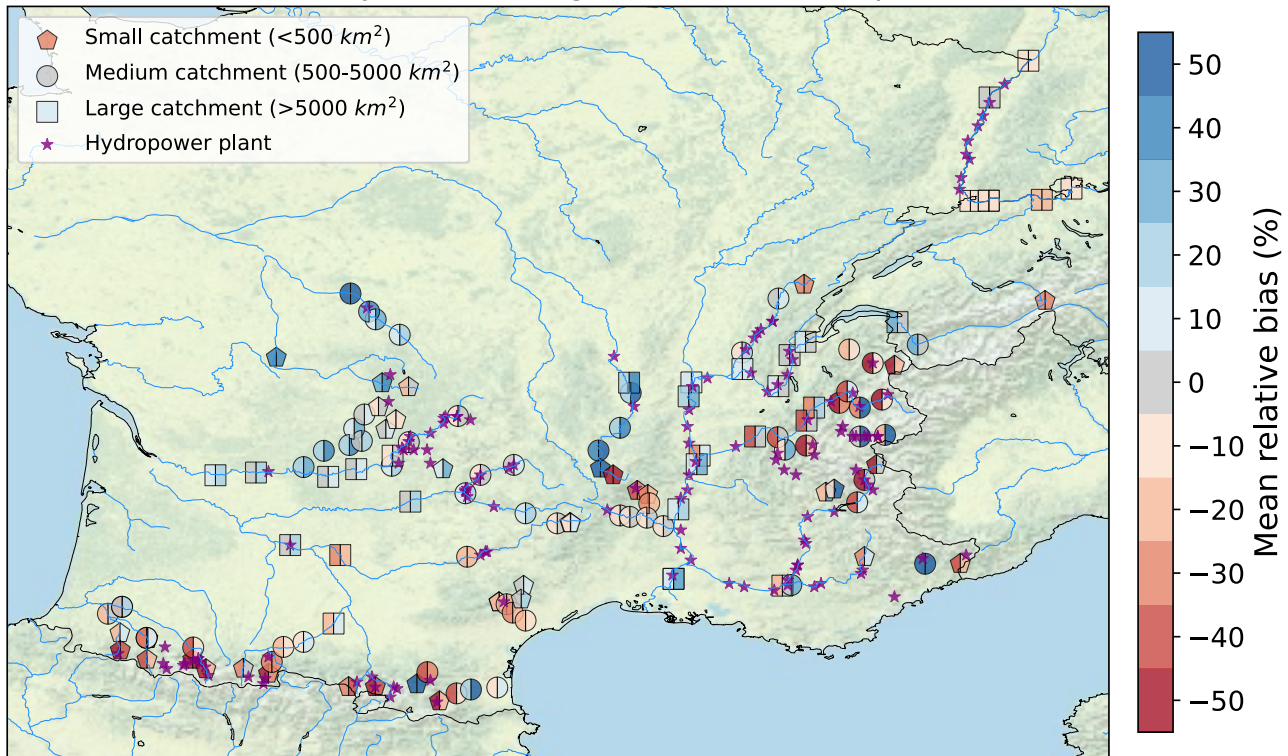


**Figure E3.** Relative bias of average in mean discharge simulated by ORCHIDEE under the alternative forcings for a selection of gauging stations located on French rivers equipped for hydropower, for the period 2010-2020. The left coloring indicated indicates the average discharge bias of discharges simulated under SAF\_COM while the right coloring indicated indicates the average discharge bias of simulations under SAF\_SPAZM.

Source: authors Authors, based on a layer by U.S. National Park Service

820 Finally, some run-of-river and poundage plants are also concentrated in the Alps, where we focus on two gauging stations: Chamonix, situated in a small upper catchment, close to a run-of-river plant and Cheylas, positioned on a large river (l'Isère), downstream from several power plants. At Chamonix, we find a seasonal bias as the model simulates an earlier discharge peak compared to observations (around 2 months ahead). At Cheylas, the model overestimates the seasonal variability of the discharge, with higher flows during Spring and lower flows during Winter, which can be attributed - at least in part - to the non-representation of reservoir management at this stage of our study (see Sect. 4.3).

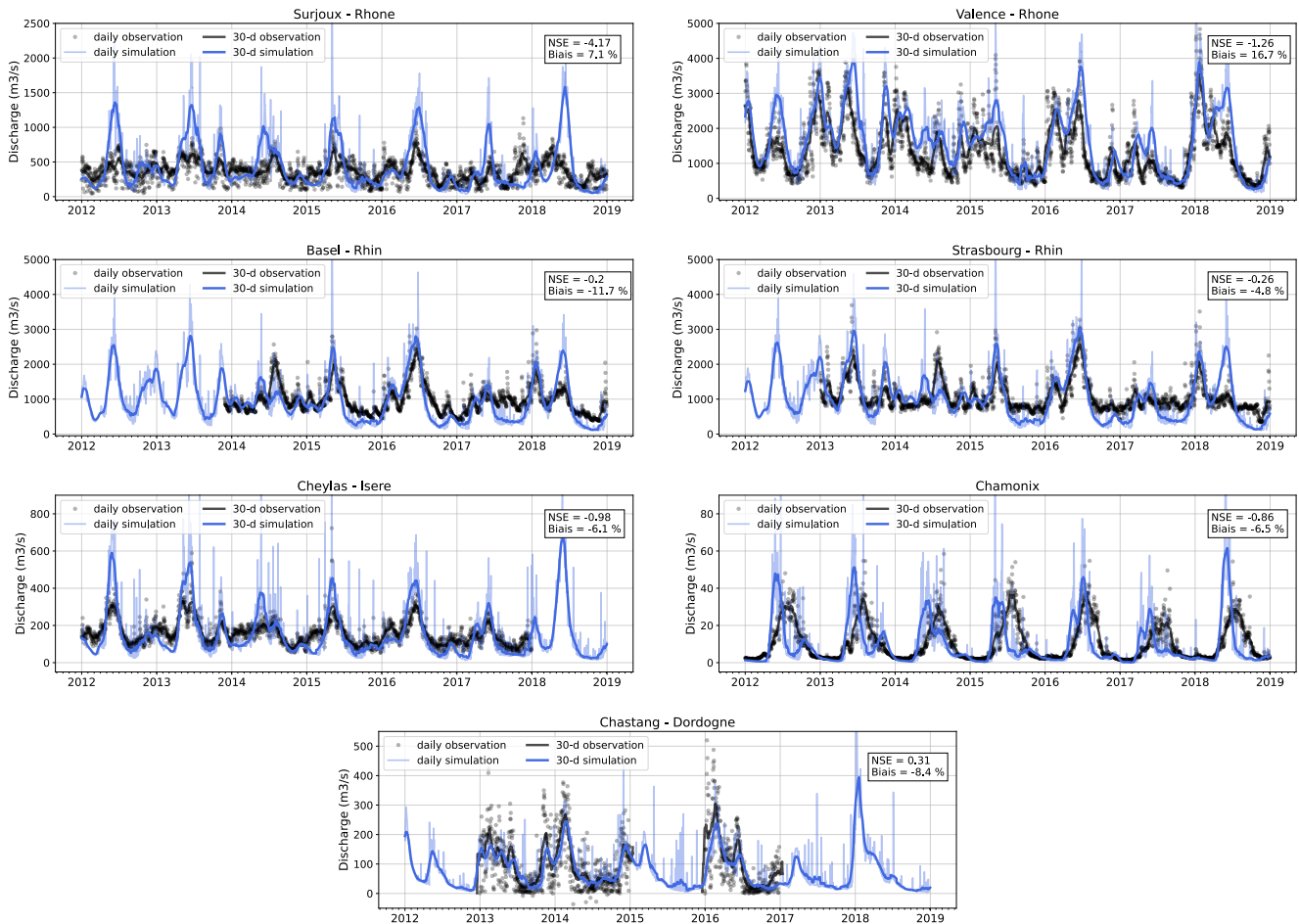


**Figure E4.** Comparison of simulated and observed river discharges for a selection of gauging stations. Locations of selected stations are indicated in Figure E1. Fines lines and dots are daily time series while ticker lines are 30-day sliding averages. NSE metrics are computed on a daily time series.

*Author contributions.* LB developed the code, designed and executed the numerical evaluations, and wrote the first draft of the manuscript. JP, PD and PQ supervised the study. All authors jointly discussed the methodology, interpreted the results and improved the manuscript.

*Competing interests.* The authors declare that they have no conflict of interest.

825 *Acknowledgements.* Baratgin's PhD is supported by the French Ministry of Agriculture. The authors are grateful to EDF-DTG for providing the SPAZM precipitation data and to Meteo-France for providing SAFRAN and COMEPHORE data. HydroPortail and ODRÉ are thanked for collecting and distributing respectively the discharge and power production data. IPSL's MesoCentre is thanked for the computer time.

## References

- Abeshu, G. W., Tian, F., Wild, T., Zhao, M., Turner, S., Chowdhury, A., Vernon, C. R., Hu, H., Zhuang, Y., Hejazi, M., et al.: Enhancing the representation of water management in global hydrological models, *Geoscientific Model Development Discussions*, pp. 1–41, 2023.
- 830 Ambec, S. and Doucet, J. A.: Decentralizing hydro power production, *Canadian Journal of Economics/Revue canadienne d'économie*, 36, 587–607, 2003.
- Birman, C., Karbou, F., Mahfouf, J.-F., Lafaysse, M., Durand, Y., Giraud, G., Mérindol, L., and Hermozo, L.: Precipitation analysis over the French Alps using a variational approach and study of potential added value of ground-based radar observations, *Journal of Hydrometeorology*, 18, 1425–1451, 2017.
- 835 CFBR: Les barrages en France, <https://www.barrages-cfbr.eu/-En-France->, 2021.
- Chowdhury, A. K., Dang, T. D., Nguyen, H. T., Koh, R., and Galelli, S.: The Greater Mekong's climate-water-energy nexus: How ENSO-triggered regional droughts affect power supply and CO2 emissions, *Earth's Future*, 9, e2020EF001 814, 2021.
- Dang, T. D., Chowdhury, A. K., and Galelli, S.: On the representation of water reservoir storage and operations in large-scale hydrological models: implications on model parameterization and climate change impact assessments, *Hydrology and Earth System Sciences*, 24, 397–416, 2020.
- 840 European Commission and Joint Research Centre (JRC): JRC Hydro-power database, <http://data.europa.eu/89h/52b00441-d3e0-44e0-8281-fda86a63546d>, 2019.
- Fekete, B. M., Wisser, D., Kroeze, C., Mayorga, E., Bouwman, L., Wollheim, W. M., and Vörösmarty, C.: Millennium ecosystem assessment scenario drivers (1970–2050): climate and hydrological alterations, *Global Biogeochemical Cycles*, 24, 2010.
- 845 François, B.: Gestion optimale d'un réservoir hydraulique multiusages et changement climatique. Modèles, projections et incertitudes: Application à la réserve de Serre-Ponçon, Ph.D. thesis, Université de Grenoble, 2013.
- Fumière, Q., Déqué, M., Nuissier, O., Somot, S., Alias, A., Caillaud, C., Laurantin, O., and Seity, Y.: Extreme rainfall in Mediterranean France during the fall: added value of the CNRM-AROME Convection-Permitting Regional Climate Model, *Climate Dynamics*, 55, 77–91, 2020.
- 850 Gottardi, F., Obled, C., Gailhard, J., and Paquet, E.: Régionalisation des précipitations sur les massifs montagneux français à l'aide de régressions locales et par types de temps, *Climatologie*, 5, 7–25, 2008.
- Habets, F., Etchevers, P., Golaz, C., Leblois, E., Ledoux, E., Martin, E., Noilhan, J., and Ottlé, C.: Simulation of the water budget and the river flows of the Rhone basin, *Journal of Geophysical Research: Atmospheres*, 104, 31 145–31 172, 1999.
- 855 Haddeland, I., Skaugen, T., and Lettenmaier, D. P.: Anthropogenic impacts on continental surface water fluxes, *Geophysical Research Letters*, 33, 2006.
- Hanasaki, N., Kanae, S., and Oki, T.: A reservoir operation scheme for global river routing models, *Journal of Hydrology*, 327, 22–41, 2006.
- Krinner, G., Viovy, N., de Noblet-Ducoudré, N., Ogée, J., Polcher, J., Friedlingstein, P., Ciais, P., Sitch, S., and Prentice, I. C.: A dynamic global vegetation model for studies of the coupled atmosphere-biosphere system, *Global Biogeochemical Cycles*, 19, 2005.
- 860 Lehner, B., Czisch, G., and Vassolo, S.: The impact of global change on the hydropower potential of Europe: a model-based analysis, *Energy Policy*, 33, 839–855, 2005.
- Lehner, B., Liermann, C. R., Revenga, C., Vörösmarty, C., Fekete, B., Crouzet, P., Döll, P., Endejan, M., Frenken, K., Magome, J., et al.: High-resolution mapping of the world's reservoirs and dams for sustainable river-flow management, *Frontiers in Ecology and the Environment*, 9, 494–502, 2011.

- 865 Lund, J. R. and Guzman, J.: Derived operating rules for reservoirs in series or in parallel, *Journal of water resources planning and management*, 125, 143–153, 1999.
- Magand, C., Ducharne, A., Tilmant, F., Le Moine, N., Sauquet, E., Mathevet, T., Vidal, J.-P., and Perrin, C.: Hybridation de réanalyses météorologiques de surface pour les zones de montagne: exemple du produit DuO sur le bassin de la Durance, *La Houille Blanche*, pp. 77–85, 2018.
- 870 Nazemi, A. and Wheeler, H. S.: On inclusion of water resource management in Earth system models, Part 1: Problem definition and representation of water demand, *Hydrology and Earth System Sciences*, 19, 33–61, <https://doi.org/10.5194/hess-19-33-2015>, 2015a.
- Nazemi, A. and Wheeler, H. S.: On inclusion of water resource management in Earth system models, Part 2: Representation of water supply and allocation and opportunities for improved modeling, *Hydrology and Earth System Sciences*, 19, 63–90, <https://doi.org/10.5194/hess-19-63-2015>, 2015b.
- 875 Neverre, N.: Rareté de l'eau et relations interbassins en Méditerranée sous changements globaux. Développement et application d'un modèle hydroéconomique à large échelle, Ph.D. thesis, Université Paris-Saclay (ComUE), 2015.
- Nguyen-Quang, T., Polcher, J., Ducharne, A., Arsouze, T., Zhou, X., Schneider, A., and Fita, L.: ORCHIDEE-ROUTING: revising the river routing scheme using a high-resolution hydrological database, *Geoscientific Model Development*, 11, 4965–4985, 2018.
- ODRÉ: Registre 2015 des installations de production raccordées au réseau de transport d'électricité, <https://www.data.gouv.fr/fr/datasets/registre-2015-des-installations-de-production-raccordees-au-reseau-de-transport-deelectricite/>, 2015.
- 880 ODRÉ: Registre 2016 des installations de production raccordées au réseau de transport d'électricité, <https://www.data.gouv.fr/fr/datasets/registre-2016-des-installations-de-production-raccordees-au-reseau-de-transport-deelectricite/>, 2016.
- ODRÉ: Registre national des installations de production et de stockage d'électricité (au 31 décembre 2018), <https://www.data.gouv.fr/fr/datasets/registre-national-des-installations-de-production-et-de-stockage-deelectricite-au-31-decembre-2018/>, 2018.
- 885 Oikonomou, K., Tarroja, B., Kern, J., and Voisin, N.: Core process representation in power system operational models: Gaps, challenges, and opportunities for multisector dynamics research, *Energy*, 238, 122 049, 2022.
- Polcher, J., Schrapffer, A., Dupont, E., Rinchiuso, L., Zhou, X., Boucher, O., Mouche, E., Otlé, C., and Servonnat, J.: Hydrological modelling on atmospheric grids; using graphs of sub-grid elements to transport energy and water, *EGUsphere*, pp. 1–34, 2023.
- Quintana-Segui, P., Le Moigne, P., Durand, Y., Martin, E., Habets, F., Baillon, M., Canellas, C., Franchisteguy, L., and Morel, S.: Analysis of near-surface atmospheric variables: Validation of the SAFRAN analysis over France, *Journal of applied meteorology and climatology*, 47, 92–107, 2008.
- 890 Ralston Fonseca, F., Craig, M., Jaramillo, P., Bergés, M., Severnini, E., Loew, A., Zhai, H., Cheng, Y., Nijssen, B., Voisin, N., et al.: Effects of climate change on capacity expansion decisions of an electricity generation fleet in the Southeast US, *Environmental Science & Technology*, 55, 2522–2531, 2021.
- 895 Reynolds, C., Jackson, T., and Rawls, W.: Estimating soil water-holding capacities by linking the Food and Agriculture Organization soil map of the world with global pedon databases and continuous pedotransfer functions, *Water Resources Research*, 36, 3653–3662, 2000.
- RTE: Generated power aggregated by sector, [https://www.services-rte.com/en/download-data-published-by-rte.html?category=generation&type=actual\\_generations\\_per\\_production\\_type](https://www.services-rte.com/en/download-data-published-by-rte.html?category=generation&type=actual_generations_per_production_type), a.
- RTE: Hydraulic stock, [https://www.services-rte.com/en/download-data-published-by-rte.html?category=generation&type=water\\_reserves](https://www.services-rte.com/en/download-data-published-by-rte.html?category=generation&type=water_reserves),
- 900 b.
- RTE, Syndicat des Energies Renouvelables, ENEDIS, ADEeF, and Agence ORE: Panorama de l'électricité renouvelable en 2016, <https://www.actu-environnement.com/media/pdf/news-28448-panorama-electricite-renouvelable-pour-annee-2016.pdf>, 2016.



- RTE, Syndicat des Energies Renouvelables, ENEDIS, ADEeF, and Agence ORE: Panorama de l'électricité renouvelable en 2018, [https://assets.rte-france.com/prod/public/2020-06/Panorama%20de%20l%27%C3%A9lectricit%C3%A9%20renouvelable%20au%2031%20decembre%202018\\_compressed.pdf](https://assets.rte-france.com/prod/public/2020-06/Panorama%20de%20l%27%C3%A9lectricit%C3%A9%20renouvelable%20au%2031%20decembre%202018_compressed.pdf), 2018.
- 905
- Schapi: HydroPortail, <https://hydro.eaufrance.fr/>, 2022.
- Siala, K., Chowdhury, A. K., Dang, T. D., and Galelli, S.: Solar energy and regional coordination as a feasible alternative to large hydropower in Southeast Asia, *Nature Communications*, 12, 4159, 2021.
- Sterl, S., Vanderkelen, I., Chawanda, C. J., Russo, D., Brecha, R. J., Van Griensven, A., van Lipzig, N. P., and Thiery, W.: Smart renewable electricity portfolios in West Africa, *Nature sustainability*, 3, 710–719, 2020.
- 910
- Stoft, S.: *Power system economics: designing markets for electricity*, vol. 468, IEEE press Piscataway, 2002.
- Tabary, P., Dupuy, P., L'Henaff, G., Gueguen, C., Moulin, L., and Laurentin, O.: A 10-year (1997—2006) reanalysis of Quantitative Precipitation Estimation over France: methodology and first results, IAHS-AISH publication, pp. 255–260, 2012.
- Turner, S. W. and Voisin, N.: Simulation of hydropower at subcontinental to global scales: a state-of-the-art review, *Environmental Research Letters*, 2022.
- 915
- Turner, S. W., Ng, J. Y., and Galelli, S.: Examining global electricity supply vulnerability to climate change using a high-fidelity hydropower dam model, *Science of the Total Environment*, 590, 663–675, 2017.
- Van Vliet, M. T., Wiberg, D., Leduc, S., and Riahi, K.: Power-generation system vulnerability and adaptation to changes in climate and water resources, *Nature Climate Change*, 6, 375–380, 2016.
- 920
- Voisin, N., Dyreson, A., Fu, T., O'Connell, M., Turner, S. W., Zhou, T., and Macknick, J.: Impact of climate change on water availability and its propagation through the Western US power grid, *Applied Energy*, 276, 115 467, 2020.
- Wagner, T., Themeßl, M., Schüppel, A., Gobiet, A., Stigler, H., and Birk, S.: Impacts of climate change on stream flow and hydro power generation in the Alpine region, *Environmental Earth Sciences*, 76, 1–22, 2017.
- Wood, A. J., Wollenberg, B. F., and Sheblé, G. B.: *Power generation, operation, and control*, John Wiley & Sons, 2013.
- 925
- Yamazaki, D. I., Jeison, S., Paul, D. B., George, H. A., and Tamlin, M. P.: MERIT Hydro: A high-resolution global hydrography map based on latest topography datasets, *Water Resources Research*, 55, 5053–5073, 2019.
- Zhou, T., Voisin, N., and Fu, T.: Non-stationary hydropower generation projections constrained by environmental and electricity grid operations over the western United States, *Environmental Research Letters*, 13, 074 035, 2018.
- Zhou, X., Polcher, J., and Dumas, P.: Representing human water management in a land surface model using a supply/demand approach, *Water Resources Research*, 57, e2020WR028 133, 2021.
- 930